A Nash Game Based Variational Model For Joint Image Intensity Correction And Registration To Deal With Varying Illumination*

Anis Theljani and Ke Chen†

Abstract. Registration aligns features of two related images so that information can be compared and/or fused in order to highlight differences and complement information. In real life images where bias field is present, this undesirable artefact causes inhomogeneity of image intensities and hence leads to failure or loss of accuracy of registration models based on minimization of the differences of the two image intensities. Here, we propose a non-linear variational model for joint image intensity correction (illumination and translation) and registration and reformulate it in a game framework. While a non-potential game offers flexible reformulation and can lead to better fitting errors, proving the solution existence for a non-convex model is non-trivial. Here we establish an existence result using the Schauder's fixed point theorem. To solve the model numerically, we use an alternating minimization algorithm in the discrete setting. Finally numerical results can show that the new model outperforms existing models.

Key words. Variational model; Optimization; Similarity measures; Mapping; Inverse Problem; Regularization procedures; Game theory; Intensity correction.

AMS subject classifications. 65M32 - 65M50 - 65M22- 94A08 - 65N22 - 35G15- 35Q68

1. Introduction.

Image registration computes a reasonable spatial geometric transformation between given images of the same object taken at different times or using different devices. It is a challenging task but, yet, a useful one in diverse fields of computational sciences and engineering such astronomy, optics, biology, chemistry, medicine and remote sensing and particularly in medical imaging. For an overview of image registration methodology and approaches, we refer to [20, 22, 33, 38, 43]. Here, we focus on development of robust variational models for deformable image registration as in the related works of ([9, 12, 15, 24, 31, 32, 48]). The usual choice of frameworks is between mono-modality (minimization of the intensity differences) and multi-modality (minimization of some non-trail functions' differences of the intensities) models. Our interested problem is somehow in between these two since an image with bias field present behaves like a different modality but the bias can introduce undesirable artefacts in registration transform, i.e., multi-modality model is not suitable since one would treat bias as features to register.

Mathematically, the image registration problem can be described as follows: Given a fixed image R, called reference and a moving image T called template which are scalar functions $T, R : \Omega \subset \mathbb{R}^d \longrightarrow \mathbb{R}$, find a reasonable geometric transformation $\varphi(\mathbf{u})(\mathbf{x}) = \mathbf{x} + \mathbf{u}(\mathbf{x})$ with $\mathbf{x},\ \mathbf{u} : \mathbb{R}^d \longrightarrow \mathbb{R}^d$ such that:

$$T[\varphi(\mathbf{u})] \equiv T(\mathbf{x} + \mathbf{u}(\mathbf{x})) \equiv T(\mathbf{u}) \approx R. \tag{1.1}$$

*EPSRC Liverpool Centre for Mathematics in Healthcare and Department of Mathematical Sciences, University of Liverpool, United Kingdom.

Funding: Both authors are supported by the UK EPSRC grant EP/N014499/1.

†Corresponding author's email: k.chen@liv.ac.uk and web: www.liv.ac.uk/cmit

(2019)

This is an equation for the unknown $\mathbf{u}$, the displacement field, which is supposed to be sought in a properly chosen functional space. The reconstruction problem based on model (1.1) is an ill-posed inverse problem and thus regularization techniques are needed to achieve well-posedness [20]. Generally, regularization consists in finding a desired displacement $\mathbf{u}$ by solving the following optimization problem:

$$\min_{\mathbf{u}\in\mathcal{H}}\{\mathcal{J}(\mathbf{u}) = S(\mathbf{u}) + \frac{\lambda}{2}D(T(\mathbf{u}), R)\} \tag{1.2}$$

where we denote by $T(\mathbf{u})$ the image $T(\mathbf{x}+\mathbf{u}(\mathbf{x}))$ and $\mathcal{H}$ is a space for the solution. The first term $S(\mathbf{u})$ is a regularization term which controls the smoothness of $\mathbf{u}$ and reflects our expectations by penalising unlikely transformations. With the aim to get more possible plausible transformations, various regularizes have been proposed, such as first-order derivatives-based on total variation [11], diffusion [18] and elastic regularizer registration models and higher-order derivatives-based on linear curvature [19], mean curvature [13] and Gaussian curvature [25].

The second term $D(T(\mathbf{u}), R)$ is a similarity measure, which quantifies distance or similarity of the transformed template image $T(\mathbf{u})$ and the reference R, whereas λ is a positive weight controlling the trade-off between them. In the case of mono-modal images, the fixed and the moving images have the similar features and the same intensity range. Thus, the L^1- distance (Sum of Absolute Differences) $D = \|T - R\|_1$ or the well-known choice L^2- distance (Sum of Squared Differences) between R and $T(\mathbf{u})$ i.e. $D = \|T - R\|_2^2$ can be used as a similarity measure.

Varying illumination. In many real life applications, even a pair of mono-modality images acquired from the same source can differ from each other, leading to inaccurate registration results. The difference is often presented as an undesirable artefact either caused by the device itself (spatially-homogeneous signal response, bias field and shading in MRI images) or caused by the imaging modality itself such as perfusion CT which creates some high contrasted regions in the image. In order to obtain accurate registration results and to cope with these problems, many models have been developed for intensity correction [1, 21, 29, 50]. It is important to note that, without intensity correction, both mono-modality and multi-modality models may fail to register the images correctly because bias introduces incorrect intensity values or false edges.

As known, the artefacts can be of either additive or multiplicative type [34, 12, 21]. It has been generally accepted that the image T with bias field, generally presented as a mixed type, relates to the 'true' unbiased image T^* via the following affine like intensity relationship: $T = mT^* + s$, where $m(\mathbf{x})$ and $s(\mathbf{x})$ are responsible for the intensity-correction. Rigorously speaking, the word 'affine' is misleading because both m, s are never constants so the model is highly non-trivial. Once m, s are found or estimated, the registration task is to find the deformation field $\mathbf{u}$ such that $T^*(\mathbf{u}) \approx R$. Denote by $T_c(\mathbf{u}) = T^*(\mathbf{u})$ the corrected and registered image of T. Hence the equivalent statement to the model $T = mT^* + s$ is

$$T(\mathbf{u}) \approx R_1 \equiv mR + s, \quad \text{since} \;\; T_c(\mathbf{u}) = \frac{T(\mathbf{u}) - s}{m} \approx R, \tag{1.3}$$

where $T(\mathbf{u})$ is the uncorrected and registered image, carrying the bias field features from T and aligned with R i.e. one may minimize one of these fidelity terms for $m, s, \mathbf{u}$ in some norm:

$$\|mR + s - T(\mathbf{u})\|, \qquad \left\|\frac{T(\mathbf{u}) - s}{m} - R\right\|.$$

We remark that any model building on minimization of the above quantities may be much simplified if one of the unknowns is dropped (i.e. $m \equiv 1$ or $s \equiv 0$); however as our tests in §5 show, a full model including both m and s always gives better results in solution quality. In fact, in many cases, intensity correction by either multiplicative or additive model is not always enough [46, 45, 41] since a combined model is necessary.

Two-stage model. To design a general-purpose registration model, a widely used approach is to make a preprocessing of the image by correcting the intensity (i.e. m, s) and then register (by $\mathbf{u}$) the corrected T^* to the reference R. The bias field and the corresponding T^* are estimated by a variational approach in deionising like fashion. The work of [28] treated m and s separately: in a pre-step, they first deal with the additive term s, referred as noise, using an additive decomposition model; see e.g. [11]. Then they proposed to minimize an energy compromised of a residual term plus regularization terms:

$$J(T^*, m) := \lambda \int_\Omega |T - mT^*|^2 d\mathbf{x} + \nu \int_\Omega |\nabla^2 m|^2 d\mathbf{x} + \kappa \int_\Omega |T^*|^2 d\mathbf{x} + \mu \int_\Omega \Phi_\epsilon(|DT^*|) d\mathbf{x}, \tag{1.4}$$

where λ, ν, κ and μ are regularization parameters and $\Phi_\epsilon(\cdot)$ is the well-known Gauss-TV penalty function.

To be precise, later, we implement a direct model aiming to find T^*, m, s, $\mathbf{u}$ by minimising by a two-stage model:

$$\text{Stage 1} \qquad \min_{T^*, m, s} J(T^*, m, s) := \lambda \int_\Omega |T - mT^* - s|^2 d\mathbf{x} + \mathcal{R}(T^*, s, m) \tag{1.5}$$

$$\text{Stage 2} \qquad \min_{\mathbf{u}} \frac{\lambda}{2} \|R - T^*(\mathbf{u})\|_2^2 + \mathcal{R}(\mathbf{u}) \tag{1.6}$$

where $\mathcal{R}(\cdot)$ contains regularization terms associated to the concerned unknowns, where different regularizes can be used. Here we have used the equivalence in (1.3).

We remark that a two-stage approach of this type is at disadvantage due to difficulties in obtaining the corrected image T^* properly. One example is the perfusion imaging modality because it is non-trivial to identify high contrast in some region as bias field or noise, and without additional information from the second image, i.e., a low contrast image, there is no way to eliminate this high contrast as it is natural in the image and it is not an obvious artefact. This can be confirmed later in numerical tests. A combined model for both intensity correction and registration seems the right approach to proceed.

Joint model. In this paper, we propose a variational approach for joint bias correction and image registration. Our first variant is the following

$$\textbf{JM} \qquad J(\mathbf{u}, m, s) := \lambda \int_\Omega |mR + s - T(\mathbf{u})|^2 d\mathbf{x} + \mathcal{R}(\mathbf{u}, s, m), \tag{1.7}$$

where $\mathcal{R}(\mathbf{u}, s, m)$ will be chosen to be the same as comparable models shortly. Since m is not a constant function, the first term in (1.7) is not convenient for numerical implementation for solving the sub-problems. Below we propose a second variant to reformulate this term. We want to transform the multiplicative term into an additive one since the latter is more convenient (a simple filtering problem). We apply a splitting method to transform the bias model (1.3) into an additive one:

$$K_l = m_l + R_l, \ \ T(\mathbf{u}) = e^{K_l} + s, \tag{1.8}$$

which is easier to handle, assuming $m, R > 0$. Here $R_l = \ln(R)$ is known since R is given, $m_l = \log(m)$, and K_l is the intermediate quantity as a spitting variable. The application of a logarithmic transform in the context of intensity transformations increases the contrast between certain intensity values [16, 10, 5, 44]. Then, our variational model takes the following form

$$\begin{aligned} \min_{\mathbf{u},s,m_l,K_l} \{ & \mathcal{L}(\mathbf{u}, s, m_l, K_l) = \\ & \mathcal{R}(\mathbf{u}, s, m_l, K_l) + \lambda_1 \int_\Omega |T(\mathbf{u}) - e^{K_l} - s|^2 d\mathbf{x} + \lambda_2 \int_\Omega |m_l + R_l - K_l|^2 d\mathbf{x} \} \end{aligned} \tag{1.9}$$

where $\mathbf{u}$ is the main deformation field variable, $\mathcal{R}(\cdot)$ contains regularization terms associated to all four unknowns (to be specified) and the rest of the energy are two fidelity terms. Here, we used the penalty method to incorporate the constraints (1.8) and alternatively we can use an augmented Lagrangian approach [6, 7]. Clearly there are no multiplicative terms in (1.9) as designed. One would normally specify $\mathcal{R}(\cdot)$ and try to solve the joint optimization problem by some techniques e.g.the alternating direction method of multipliers (ADMM) [7]. The problem (1.9) will be split into 4 sub-problems for each of the main variables: $\mathbf{u}, s, m_l, K_l$. There are two challenges: i) choosing the 5 parameters (assuming there are 3 new parameters from $\mathcal{R}(\cdot)$) suitably is a highly non-trivial task; ii) one cannot avoid coupling all 4 variables in any sub-problem.

However, we like to reformulate it to another form using the Nash game idea where both of these two challenges are overcome: first, each sub-problem will have one parameter which can be tuned for that sub-problem in an easier way; second, we can modify the above sub-problems to reduce couplings and hence improve convergence. Accompanied with these advantages, unfortunately, we have two emerging questions: (i) the optimization energy is implicitly modified so the new minimizers may not be the same as for the original model – which is better? (ii) how to show that the game based reformulation has a solution? We shall demonstrate that the game model offers a better solution for two main aspects: choice of underlying parameters and proof of solution existence. In fact, the K_l sub-problem in model (1.9) has three terms and involves two penalty parameters λ_1 and λ_2, which are pretended to be large enough. The solution will be sensitive to these two parameters and the optimal choice is non-trivial. We shall reformulate this problem to yield only one parameter (instead of two) by considering a game approach that has a separable structure in the sense that it is not very sensible these weights.

In game approach, the proof of existence of an equilibrium solution is generally challenging for non-convex functions (though easy for convex ones).

Nash game terminology. We consider a game with four energies $\mathcal{J}_i(\cdot)$, one for each player i indexed by $i \in \{1,\dots,4\}$, which are written in the following form

$$\mathcal{J}_i(p_1,p_2,p_3,p_4) = \mathcal{R}_i(p_i) + \mathcal{G}_i(p_1,p_2,p_3,p_4)$$

where $\mathcal{G}_i(\cdot)$ represents the individual penalty of player "i" depending on the strategies of all players and $\mathcal{R}_i$ is a convex penalty for player "i" .

Definition 1.1. *A quadruplet $\mathbf{z}_N = (p_1^*,p_2^*,p_3^*,p_4^*) \in X_1 \times X_2 \times X_3 \times X_4$ is called Nash equilibrium [36] for the four-players game involving the costs $\mathcal{J}_i(\cdot)$ $(i=1,\dots,4)$ if the following inequalities hold*

$$\begin{cases} \mathcal{J}_1(p_1^*,p_2^*,p_3^*,p_4^*) \le \mathcal{J}_1(p_1,p_2^*,p_3^*,p_4^*), \ \forall p_1 \in X_1, \\ \mathcal{J}_2(p_1^*,p_2^*,p_3^*,p_4^*) \le \mathcal{J}_2(p_1^*,p_2,p_3^*,p_4^*), \ \forall p_2 \in X_2, \\ \mathcal{J}_3(p_1^*,p_2^*,p_3^*,p_4^*) \le \mathcal{J}_3(p_1^*,p_2^*,p_3^*,p_4^*), \ \forall p_3 \in X_3, \\ \mathcal{J}_4(p_1^*,p_2^*,p_3^*,p_4^*) \le \mathcal{J}_4(p_1^*,p_2^*,p_3^*,p_4), \ \forall p_4 \in X_4. \end{cases}$$

Observe that, to achieve equilibrium in an algorithmic fashion, each optimization has one variable to minimize; if each one optimizes with respect to all 4 variables, there will be at least 4 unrelated (respective) solutions to compete to each other – hence a game. As remarked, existence of a Nash equilibrium in non-potential games can be easily obtained by applying the Nash theorem if each energy $\mathcal{G}_i(\cdot)$ is convex w.r.t the variables p_i [37]. For important techniques and results in game theory and its connections to partial differential equations (PDEs) for other problems, the reader is directed to [23, 26, 27, 42].

The rest of the paper is organized as follows: Section 2 is devoted to the introduction of the proposed Nash game strategy approach with four strategies. Section 3 addresses the mathematical analysis of the proposed model as well as the proof of the existence of Nash equilibrium. Section 4 is dedicated to the numerical study. We first propose the iterative numerical algorithm used to find a **Nash equilibrium** [37] and then prove its convergence. Finally, Section 5 concerns the implementation and the presentation of several numerical examples to test the efficiency and robustness of the proposed approach in comparison with existing models.

2. Nash game based reformulation of our registration model and its theory.

In this section, we formulate our second variant (1.9) of a joint model as a game involving four players and seek its solution as a **Nash equilibrium**. We discuss the characterization of this equilibrium solution and prove its existence. We define the players in our problem by $(p_1,p_2,p_3,p_4) = (\mathbf{u}, s, m_l, K_l)$ in the space $\mathcal{X} = \mathcal{W} \times W^{1,2}(\Omega) \times W^{1,2}(\Omega) \times W^{1,2}(\Omega)$ where $\mathcal{W} = W^{2,2}(\Omega,\mathbb{R}^2) \cap W_0^{1,2}(\Omega,\mathbb{R}^2)$. The space $\mathcal{X}$ is endowed with the following norm

$$\|\mathbf{z}\|_{\mathcal{X}} = \left(\|\mathbf{u}\|_{\mathcal{W}}^2 + \|\nabla s\|_{W^{1,2}(\Omega)}^2 + \|\nabla m_l\|_{W^{1,2}(\Omega)}^2 + \|\nabla K_l\|_{W^{1,2}(\Omega)}^2\right)^{1/2},$$

where $\|\mathbf{u}\|_{\mathcal{W}} = \left(\|\nabla \mathbf{u}\|_2^2 + \|\nabla^2 \mathbf{u}\|_2^2\right)^{1/2}$. The game formulation allows many choices of energies $\mathcal{R}_i(\cdot)$ and $\mathcal{G}_i(\cdot)$ whose terms may not be part of each other. The choice of the different energies leads to either potential or non-potential games [35]. The potential game structure is very important because it makes easy to prove the existence of Nash equilibrium [37, 36]. One example is to make the particular choice of the following energies $\mathcal{J}_i(\cdot) = \mathcal{R}_i(\cdot) + \mathcal{G}_i(\cdot)$ with

$$(2.1) \qquad \begin{cases} \mathcal{R}_1(\mathbf{u}) = \|\mathbf{u}\|_{\mathcal{W}}^2, & \mathcal{G}_1(\mathbf{u}, s, m_l, K_l) = \lambda_1 \int_\Omega |T(\mathbf{u}) - e^{K_l} - s|^2 d\mathbf{x}, \\ \mathcal{R}_2(s) = \int_\Omega |\nabla s|^2 \, d\mathbf{x}, & \mathcal{G}_2(\mathbf{u}, s, m_l, K_l) = \lambda_2 \int_\Omega |T(\mathbf{u}) - e^{K_l} - s|^2 d\mathbf{x}, \\ \mathcal{R}_3(m_l) = \int_\Omega |\nabla m_l|^2 \, d\mathbf{x}, & \mathcal{G}_3(\mathbf{u}, s, m_l, K_l) = \lambda_3 \int_\Omega |m_l + R_l - K_l|^2 d\mathbf{x}, \\ \mathcal{R}_4(K_l) = \int_\Omega |\nabla K_l|^2 \, d\mathbf{x}, & \mathcal{G}_4(\mathbf{u}, s, m_l, K_l) = \lambda_4 \int_\Omega |m_l + R_l - K_l|^2 d\mathbf{x} \\ & \qquad + \lambda_5 \int_\Omega |T(\mathbf{u}) - e^{K_l} - s|^2 d\mathbf{x}, \end{cases}$$

where $\mathcal{R}_i(\cdot)$ is the regularization term in energy i. There are many possible choices of regularization leading to different solution spaces. For the deformation $\mathbf{u}$, we use regularizes based on combined first and second-order derivatives. Using only the first-order derivatives, i.e., H^1 semi-norm, is sensitive to affine pre-registration. We avoid this problem by combining it with the second-order derivative term which are not sensitive to (affine) pre-registration as it has the affine transformations in its kernel. Moreover, this choice penalizes oscillations and also allows smooth transformations in order to get visually pleasing registration results. The variables K_l, m_l and s are chosen in the space $W^{1,2}(\Omega)$ and we could consider different spaces such as $W^{2,2}(\Omega)$ or the space of bounded variation functions $BV(\Omega)$.

The formulation in (2.1) is special cases of game formulation known as a potential game (**PG**) [35] which amounts to find a minimizer of an energy $\mathcal{L}(\cdot) = \sum_i^4 \mathcal{J}_i(\mathbf{u}, s, m_l, K_l)$ in (1.9) – then the game model reduces to an ADMM algorithm if alternating iterations are used or a Nash equilibrium of (1.9) is a minimizer of $\sum_i^4 \mathcal{J}_i(\mathbf{u}, s, m_l, K_l)$. We refer the reader to [35, 4, 2] for more details about potential game in PDEs .

In this work, instead of (2.1), we modify $\mathcal{J}_3, \mathcal{J}_4$ new sub-problems which lead to a better model than (2.1); our new energies to be minimized are still denoted by $\mathcal{J}_i = \mathcal{R}_i + \mathcal{G}_i$, for $i = 1, 2, 3, 4$, with all terms defined in (2.1) except these 3 new terms i.e.

$$(2.2) \qquad \begin{cases} \mathcal{R}_1(\mathbf{u}) = \|\mathbf{u}\|_{\mathcal{W}}^2, \quad \mathcal{G}_1(\mathbf{u}, s, m_l, K_l) = \lambda_1 \int_\Omega |T(\mathbf{u}) - e^{K_l} - s|^2 d\mathbf{x}, \\ \mathcal{R}_2(s) = \int_\Omega |\nabla s|^2 \, d\mathbf{x}, \quad \mathcal{G}_2(\mathbf{u}, s, m_l, K_l) = \lambda_2 \int_\Omega |T(\mathbf{u}) - e^{K_l} - s|^2 d\mathbf{x}, \\ \mathcal{R}_3(m_l) = \int_\Omega |\nabla m_l|^2 \, d\mathbf{x}, \quad \mathcal{G}_3(\mathbf{u}, s, m_l, K_l) = \lambda_3 \int_\Omega |m_l + R_l - \ln(T(\mathbf{u}) - s)|^2 d\mathbf{x}, \\ \mathcal{R}_4(K_l) = \int_\Omega |\nabla K_l|^2 \, d\mathbf{x} + \iota_A(K_l), \quad \mathcal{G}_4(\mathbf{u}, s, m_l, K_l) = \lambda_4 \int_\Omega |m_l + R_l - K_l|^2 d\mathbf{x}, \end{cases}$$

where $A = \{K_l \in L^2(\Omega); K_{\min} \leq K_l \leq K_{\max}\}$ is a closed and convex set and $\iota_A(\cdot)$ is a projection into A. The variables K_l is bounded for theoretical reasons in order to prove the existence of a Nash equilibrium. In this case, a Nash equilibrium is not a minimizer of $\sum_i^4 \mathcal{J}_i(\mathbf{u}, s, m_l, K_l)$, which makes difficult the proof of the existence. Formally this Nash game problem is called a non-potential game (denoted by **NPG**). Clearly the essential simplification is in $\mathcal{G}_4$ and there are other possible alternative formulations e.g. using L_1 semi-norm. These changes simplify the K_l-problem in (2.1), equivalently in (1.9), where the K_l-energy has three terms and which necessitates two regularization parameters λ_4 and λ_5. Whereas, in the game approach (2.2), the same problem consists only of regularization and one fidelity term, i.e., has only one parameter λ_4. Moreover, to discuss any theory for (2.2), we have to address the non-convexity e.g. the energy $\mathcal{G}_1(\cdot)$ is non-convex w.r.t $\mathbf{u}$. Non-convexity means that we cannot apply the Nash theorem [37] to show the existence of a Nash equilibrium. To overcome this challenge, we take the inclusion approaches below.

2.1. Existence of Nash equilibrium. To establish the existence of a Nash equilibrium for model (2.2), we take a monotone operator method for solving an auxiliary monotone inclusion problem [14], whose solutions are Nash equilibria [8]. We define the following two operators to incorporate gradients of our four energies $\{\mathcal{J}_i\}$:

$$\mathbf{A} = (\nabla\mathcal{R}_1, \nabla\mathcal{R}_2, \nabla\mathcal{R}_3, \nabla\mathcal{R}_4), \quad \mathbf{B} = (\nabla_{p_1}\mathcal{G}_1, \nabla_{p_2}\mathcal{G}_2, \nabla_{p_3}\mathcal{G}_3, \nabla_{p_1}\mathcal{G}_4). \tag{2.3}$$

Then, the quadruplet $\mathbf{z} = (p_1, p_2, p_3, p_4) = (\mathbf{u}, s, m_l, K_l)$ is a Nash equilibrium for our game involving the four energies $\{\mathcal{J}_i(\cdot)\}$, if it solves the inclusion problem

$$\mathbf{z} \in ker(\mathbf{A} + \mathbf{B}). \tag{2.4}$$

The fact that $\mathbf{z}$ is a Nash equilibrium can be seen from

$$\mathbf{z} \in ker(\mathbf{A} + \mathbf{B}) \Leftrightarrow \mathbf{B}(\mathbf{z}) \in -\mathbf{A}(\mathbf{z}) \Longleftrightarrow \begin{cases} \nabla_{p_1}\mathcal{G}_1(\mathbf{z}) \in \nabla\mathcal{R}_1(\mathbf{z}), \\ \nabla_{p_2}\mathcal{G}_2(\mathbf{z}) \in \nabla\mathcal{R}_2(\mathbf{z}), \\ \nabla_{p_3}\mathcal{G}_3(\mathbf{z}) \in \nabla\mathcal{R}_3(\mathbf{z}), \\ \nabla_{p_4}\mathcal{G}_4(\mathbf{z}) \in \nabla\mathcal{R}_4(\mathbf{z}). \end{cases}$$

We consider the inclusion problem (2.4) by solving the following system

$$\begin{cases} -\Delta u_1 + \mathrm{div}^2[\nabla^2 u_1] & = \lambda_1(T(\mathbf{u}) - e^{K_l} - s)\partial_x T(\mathbf{u}), \\ -\Delta u_2 + \mathrm{div}^2[\nabla^2 u_2] & = \lambda_1(T(\mathbf{u}) - e^{K_l} - s)\partial_y T(\mathbf{u}), \\ -\ \Delta s + \lambda_2 s & = \lambda_2 T(\mathbf{u}) - \lambda_2 e^{K_l}, \\ -\Delta m_l + \lambda_3 m_l & = \lambda_3 \ln(T(\mathbf{u}) - s) - \lambda_3 R_l, \\ -\Delta K_l + \lambda_5 K_l + p & = \lambda_4(m_l + R_l), \end{cases} \tag{2.5}$$

where $p \in \partial\iota_A(K_l)$. In general, the existence of solution in (2.5) is guaranteed if the operator $\mathbf{B}$ is monotone; such a property is not true in our case due to non-convexity. Therefore, we prove the existence of Nash equilibrium for the **NPG** game (2.2) by using a fixed point methodology. We introduce the operator $\mathcal{T}(\mathbf{u}, s) = (\mathbf{v}, h) : (L^2(\Omega))^2 \times L^2(\Omega) \longrightarrow (L^2(\Omega))^2 \times L^2(\Omega)$ defined by the following auxiliary system of PDEs

$$\begin{cases} -\Delta v_1 + \mathrm{div}^2[\nabla^2 v_1] & = \lambda_1(T(\mathbf{u}) - e^{K_l} - h)\partial_x T(\mathbf{u}), \\ -\Delta v_2 + \mathrm{div}^2[\nabla^2 v_2] & = \lambda_1(T(\mathbf{u}) - e^{K_l} - h)\partial_y T(\mathbf{u}), \\ -\ \Delta h + \lambda_2 h & = \lambda_2 T(\mathbf{u}) - \lambda_2 e^{K_l}, \\ -\Delta m_l + \lambda_3 m_l & = \lambda_3 \ln(T(\mathbf{u}) - s) - \lambda_3 R_l, \\ -\Delta K_l + \lambda_4 K_l + p & = \lambda_4(m_l + R_l), \end{cases} \tag{2.6}$$

where p is an element of the sub-differential of $\iota_A(K_l)$, i. e., $p \in \partial\iota_A(K_l)$. Now, we show that such a definition is well posed.

Proposition 2.1. *For any given $(\mathbf{u}, s) \in (L^2(\Omega))^2 \times L^2(\Omega)$, there exists a unique weak solution $\mathbf{z} = (\mathbf{v}, h, m_l, K_l)$ for the system (2.6).*

Proof. The system (2.6) is written in the following form

$$-\mathbf{N}(\mathbf{z}) \in \mathbf{M}(\mathbf{z}), \tag{2.7}$$

where

$$\mathbf{M}(\mathbf{z}) = \mathbf{A}(\mathbf{z}) + \begin{pmatrix} 0 \\ 0 \\ \lambda_2 \\ \lambda_3 \\ 0 \end{pmatrix} \cdot \mathbf{z}, \; \mathbf{N}(\mathbf{z}) = \begin{pmatrix} -\lambda_1(T(\mathbf{u}) - e^{K_l} - h)\partial_x T(\mathbf{u}) \\ -\lambda_1(T(\mathbf{u}) - e^{K_l} - h)\partial_y T(\mathbf{u}) \\ -\lambda_2 T(\mathbf{u}) + \lambda_2 e^{K_l} \\ -\lambda_3 \ln(T(\mathbf{u}) - s) + \lambda_3 R_l \\ \lambda_4 K_l - \lambda_4(m_l + R_l) \end{pmatrix} \text{ and } \mathbf{z} = \begin{pmatrix} v_1 \\ v_2 \\ h \\ m_l \\ K_l \end{pmatrix}. \tag{2.8}$$

where the operator $\mathbf{A}$ is given in (2.3). Moreover, we easy verify that $(\mathbf{N}(\mathbf{z}) - \mathbf{N}(\mathbf{z}') \cdot (\mathbf{z} - \mathbf{z}') \geq 0$, which means that the operator $\mathbf{N}$ is monotone; we see that the first three PDEs are strictly elliptic. On the other hand, since the operator $\mathbf{M}$ is maximally monotone in the space $\mathcal{X}$, the system (2.6) has a unique solution $\mathbf{z}$ [14]. ∎

Note that whenever there exists a fixed point $(\mathbf{u}, h)$ for operator $\mathcal{T}(\cdot)$, the quadruplet $(\mathbf{u}, h, m_l, K_l)$ will be a solution for the inclusion problem (2.5). We are ready to state a main result for our model (2.6).

Proposition 2.2. *There exists $C > 0$ such that $\mathcal{T} : B(0, C) \longrightarrow B(0, C)$ is is continuous and compact, where $\mathcal{T}$ is the operator from (2.6) and $B(0, C)$ is the convex and closed ball in $(L^2(\Omega))^2 \times L^2(\Omega)$ of radius C. Hence $\mathcal{T}$ admits a fixed point and consequently model (2.2) admits a solution $\mathbf{z}$.*

Proof. Existence of C. Multiplying the first, second and third equations by v_1, v_2 and h, respectively, we get

$$\begin{aligned}
\|v_1\|_2^2 &\leq \lambda_1 \|T(\mathbf{u})\partial_x T(\mathbf{u})\|_2 \|v_1\|_2 + \lambda_1 \|e^{K_l} \partial_x T(\mathbf{u})\|_2 \|v_1\|_2 + \lambda_1 \|h \partial_x T(\mathbf{u})\|_2 \|v_1\|_2, \\
\|v_2\|_2^2 &\leq \lambda_1 \|T(\mathbf{u})\partial_y T(\mathbf{u})\|_2 \|v_2\|_2 + \lambda_1 \|e^{K_l} \partial_y T(\mathbf{u})\|_2 \|v_2\|_2 + \lambda_1 \|h \partial_y T(\mathbf{u})\|_2 \|v_2\|_2, \\
\|h\|_2^2 &\leq \lambda_2 \|T(\mathbf{u})\|_2 \|h\|_2 + \lambda_2 \|e^{K_l}\|_2 \|h\|_2.
\end{aligned}$$

As both the image T and its gradient $\nabla T(\cdot)$ are assumed to be bounded, and $\mathbf{u} \in \mathcal{X}$, i.e., continuous, we have that $T(\mathbf{u})$ and $\nabla T(\mathbf{u})$ are bounded and

$$\|v_1\|_2 \leq C_1(\|T(\mathbf{u})\|_2 + \|e^{K_l}\|_2 + \|h\|_2), \tag{2.9}$$

$$\|v_2\|_2 \leq C_2(\|T(\mathbf{u})\|_2 + \|e^{K_l}\|_2 + \|h\|_2), \tag{2.10}$$

$$\|h\|_2 \leq \lambda_2(\|T(\mathbf{u})\|_2 + \|e^{K_l}\|_2), \tag{2.11}$$

where $C_1, C_2 > 0$ depend on $\nabla T(\cdot)$. Moreover, we have $K_{min} \leq K_l \leq K_{max}$ since K_l is the unique solution of

$$\arg\min_{K_l} \int_\Omega |\nabla K_l|^2 \, dx + \lambda_4 \int_\Omega |m_l + R_l - K_l|^2 dx + \iota_A(K_l).$$

Thus, using the fact that $K_{min} \leq K_l \leq K_{max}$ and $\nabla T(\cdot)$ is bounded, we get from the inequality (2.11) that $\|h\|_2 \leq c$ for a constant $c > 0$. Moreover, from the inequalities (2.9) and (2.10), we also get that $\|\mathbf{v}\|_2 \leq c_1$ where $c_1 > 0$ is a constant. Thus, have

$$\|(\mathbf{v}, h)\|_2 \leq C,$$

where C is a constant depending on T, ∇T, K_{max} and K_{min}. Then, we conclude that the operator maps from $B(0, C)$ into itself, where $B(0, C)$ is the closed ball in $(L^2(\Omega))^2 \times L^2(\Omega)$ of radius C, i.e., $\mathcal{T} : B(0, C) \longrightarrow B(0, C)$.

Compactness of $\mathcal{T}$. As the injection from the product space $\mathcal{W}(\Omega) \times W^{1,2}(\Omega)$ into the space $(L^2(\Omega))^2 \times L^2(\Omega)$ is compact, the operator $\mathcal{T} : B(0, C) \longrightarrow B(0, C)$ is then compact.

Continuity of $\mathcal{T}$. Let $(\mathbf{u}_n, s_n)_{n\geq 0}$ be a sequence in $B(0, C)$ which converges to $(\mathbf{u}, s)$ and $(\mathbf{v}_n, h_n) = \mathcal{T}(\mathbf{u}_n, s_n)$. Then, from the definition of the operator $\mathcal{T}(\cdot)$, $(\mathbf{v}_n, h_n)$ fulfils the following system of PDEs

$$(2.12) \qquad \begin{cases} -\Delta v_1^n + \operatorname{div}^2[\nabla^2 v_1^n] & = \lambda_1(T(\mathbf{u}^n) - e^{{K_l}^n} - h^n)\partial_x T(\mathbf{u}^n), \\ -\Delta v_2^n + \operatorname{div}^2[\nabla^2 v_2^n] & = \lambda_1(T(\mathbf{u}^n) - e^{{K_l}^n} - h^n)\partial_y T(\mathbf{u}^n), \\ -\Delta h^n + \lambda_2 h^n & = \lambda_2 T(\mathbf{u}^n) - \lambda_2 e^{{K_l}^n}, \\ -\Delta {m_l}^n + \lambda_3 m_{ln} & = \lambda_3 \ln(T(\mathbf{u}^n) - s^n) - \lambda_3 R_l, \\ -\Delta {K_l}^n + \lambda_5 {K_l}^n + p^n & = \lambda_4({m_l}^n + R_l), \end{cases}$$

where $p^n \in \partial\iota_A({K_l}^n)$. Since $(\mathbf{u}^n, s^n) \in B(0, C) \times B(0, C)$ and image $T(\cdot)$ is bounded, we get that $({m_l}^n)_n$ is uniformly bounded in $W^{1,2}(\Omega)$ from the fourth equation of system (2.12). Furthermore, we have

$$\|K_{ln}\|_{W_0^{1,2}(\Omega)} \leq cJ_4(K_{ln}) \leq c\mathcal{J}(K_{min}) = c\lambda_4 \int_\Omega |m_{ln} + R_l - K_{min}|^2 dx,$$

where $c > 0$. Since $({m_l}^n)_n$ is uniformly bounded in $W^{1,2}(\Omega)$, we get that $({K_l}^n)_n$ is also bounded in $W^{1,2}(\Omega)$. The last equation in the system (2.12) combined with the boundedness of $({K_l}^n)_n$ in $W^{1,2}(\Omega)$ and $({m_l}^n)_n$ in $L^2(\Omega)$ give that $(p^n)_n$ is bounded in $L^2(\Omega)$. Using classical stability estimates for elliptic PDEs for the three first equations in system (2.12) and the fact that $K_{min} \leq K_l \leq K_{max}$, $T(\cdot)$ and $\nabla T(\cdot)$ are bounded, we obtain that $(\mathbf{v}^n)_n$ and $(h^n)_n$ are uniformly bounded in the spaces $\mathcal{W}$ and $W^{1,2}(\Omega)$, respectively. Thus, we can extract a subsequence $(\mathbf{v}^n)_n$, $(h^n)_n$, $({m_l}^n)_n$, $({K_l}^n)_n$ and $(p^n)_n$ such that $\mathbf{v}^n \rightharpoonup \mathbf{v}$ weakly in $\mathcal{W}(\Omega)$, $h^n \rightharpoonup h$ weakly in $W^{1,2}(\Omega)$, ${m_l}^n \rightharpoonup m_l$ weakly in $W^{1,2}(\Omega)$, ${K_l}^n \rightharpoonup K_l$ weakly in $W^{1,2}(\Omega)$ and $p^n \rightharpoonup p$ weakly in $L^2(\Omega)$ where $p \in \partial\iota_A(K_l)$, as n goes to $+\infty$. It follows that the limit $(\mathbf{v}, h, m_l, K_l)$ is a weak solution of the system (2.6). Therefore, from the uniqueness of a weak solution for the system (2.6) in Proposition 2.1, we have $\mathcal{T}(\mathbf{u}, s) = (\mathbf{v}, h)$. Thus, we conclude that $\mathcal{T}(\cdot)$ is continuous in $B(0, C)$.

Existence. Finally to complete the proof, applying the Schauder's fixed-point theorem [17] and from the above properties, we see that $\mathcal{T}$ admits a fixed point, which implies that the inclusion problem (2.5) admits a solution $\mathbf{z}$. Consequently this quadruplet $\mathbf{z}$ is also a solution to model (2.2). ∎

3. Iterative algorithm.

To compute a Nash equilibrium, we use an alternating forward-Backward algorithm (ADMM like) [3, 14], by means of an iterative process and proximal operators [40]. We first discuss the discretization step.

3.1. Discretization.

The given images R, T and the displacement fields $\mathbf{u}$ are discretized on a uniform mesh by vertex centred discretization. We assume that the images have $p \times q$ pixels, where p and q are the numbers of rows and columns in the image, respectively. So the discrete solution $\mathbf{u}^{i,j} = (u_1(x_i, y_j), u_2(x_i, y_j))$, $i = 1, \cdots, p$, $j = 1, \cdots, q$. Other quantities are set up similarly.

For sake of simplicity, we use a generic notation u for discussing discretization. For the discrete differential operators, we assume periodic boundary conditions for u. Then, the action of each of the discrete differential operators can be regarded as a circular convolution of u and allows the use of fast Fourier transform (see [39, 47, 49] for more details). The discrete gradient is an operator from $\mathbb{R}^{p\times q}$ to $\mathbb{R}^{p\times q} \times \mathbb{R}^{p\times q}$ and given by $\nabla u = (\partial_x u, \partial_y u)$ where $\partial_x u$ and $\partial_y u$ are *forward* difference operators defined as follows:

$$\partial_x u = \begin{cases} u(i+1,j) - u(i,j), & 1 \le i < p, 1 \le j \le q, \\ u(1,j) - u(i,j), & i = p, 1 \le j \le q, \end{cases}$$

$$\partial_y u = \begin{cases} u(i,j+1) - u(i,j), & 1 \le i \le p, 1 \le j < q, \\ u(i,1) - u(i,j), & 1 \le i \le p, j = q. \end{cases}$$

The discrete divergence is an operator from $\mathbb{R}^{p\times q} \times \mathbb{R}^{p\times q}$ to $\mathbb{R}^{p\times q}$, for $\mathbf{n} = (n_1, n_2)$, is given by *backward* difference operators: $\operatorname{div} \mathbf{n} = \overleftarrow{\partial}_x n_1 + \overleftarrow{\partial}_y n_2$ where

$$\overleftarrow{\partial}_x u = \begin{cases} u(i,j) - u(i-1,j), & 1 < i \le p,\ 1 \le j \le q, \\ u(i,j) - u(p,j), & i = 1,\ 1 \le j \le q, \end{cases}$$

$$\overleftarrow{\partial}_y u = \begin{cases} u(i,j) - u(i,j-1), & 1 \le i \le p,\ 1 < j \le q, \\ u(i,j) - u(i,q), & 1 \le i \le p,\ j = 1, \end{cases}$$

are backward difference operators. Then, the discrete Laplace operator is given by $\Delta u = \operatorname{div}(\nabla u)$. Similarly, we define the second-order discrete differential operators:

$$\partial_{xx} u = \overleftarrow{\partial}_{xx} u = \begin{cases} u(p,j) - 2u(i,j) + u(i+1,j), & i = 1, 1 \le j \le q, \\ u(i-1,j) - 2u(i,j) + u(i+1,j), & 1 < i < p, 1 \le j \le q, \\ u(i-1,j) - 2u(i,j) + u(1,i), & i = p, 1 \le j \le q. \end{cases}$$

$$\partial_{yy} u = \overleftarrow{\partial}_{yy} u = \begin{cases} u(i,q) - 2u(i,j) + u(i,j+1), & 1 \le i \le p,\ j = 1, \\ u(i,j-1) - 2u(i,j) + u(i,j+1), & 1 \le i \le p,\ 1 < j < q, \\ u(i,j-1) - 2u(i,j) + u(i,1), & 1 \le i \le p,\ j = q. \end{cases}$$

$$\partial_{xy} u = \partial_{yx} u = \begin{cases} u(i,j) - u(i+1,j) - u(i,j+1) + u(i+1,j+1), & 1 \le i < p, 1 \le j < q, \\ u(i,j) - u(1,j) - u(i,j+1) + u(1,j+1), & i = p, 1 \le j < q, \\ u(i,j) - u(i+1,j) - u(i,1) + u(i+1,1), & 1 \le i < p, j = q, \\ u(i,j) - u(1,j) - u(i,1) + u(1,1), & i = p, j = q. \end{cases}$$

$$\overleftarrow{\partial}_{xy} u = \overleftarrow{\partial}_{yx} u \begin{cases} u(i,j) - u(i,q) - u(p,j) + u(l,cq), & i = p, j = 1, \\ u(i,j) - u(i,j-1) - u(p,j) + u(p,j-1), & i = 1, 1 \le j < q, \\ u(i,j) - u(i,q) - u(i-1,j) + u(i-1,q), & 1 < i < p, j = 1, \\ u(i,j) - u(i,j-1) - u(i-1,j) + u(i-1,j-1), & 1 < i < p, 1 < j \le q. \end{cases}$$

Based on the above operators, we define the following fourth-order differential operator:

$$\mathrm{div}^2[\nabla^2 u] = \overleftarrow{\partial}_{xx}\partial_{xx}u + \overleftarrow{\partial}_{yy}\partial_{yy}u + \overleftarrow{\partial}_{xy}\partial_{xy}u + \overleftarrow{\partial}_{yx}\partial_{yx}u.$$

3.2. Solution of sub-problems.

In this section, we present an iterative solution algorithm for all four discrete sub-problems in Algorithm 3.1. The efficiency is achieved by the use of the FFT-transform.

Algorithm 3.1 Forward-Backward algorithm for computing a Nash equilibrium

- Set $k = 0$ and choose an initial guess $\mathbf{z}^{(0)} = (\mathbf{u}^{(0)}, s^{(0)}, {m_l}^{(0)}, {K_l}^{(0)})$.
- Step 1: Compute (in parallel) $(\mathbf{u}^{(k+1)}, s^{(k+1)}, {m_l}^{(k+1)}, {K_l}^{(k+1)})$ solution of

$$\overline{\mathbf{u}}^{(k)} = \mathbf{u}^k - \gamma\nabla\mathcal{G}_{p_1}(\mathbf{u}^k, s^k, {m_l}^k, {K_l}^k), \qquad \mathbf{u}^{(k+1)} = \mathbf{prox}_{\gamma\mathcal{R}_1}(\overline{\mathbf{u}}^{(k)}) \tag{3.1}$$

$$\overline{s}^{(k)} = s^k - \gamma\nabla\mathcal{G}_{p_2}(\mathbf{u}^k, s^k, {m_l}^k, {K_l}^k), \qquad s^{(k+1)} = \mathbf{prox}_{\gamma\mathcal{R}_2}(\overline{s}^{(k)}) \tag{3.2}$$

$$\overline{m_l}^{(k)} = {m_l}^k - \gamma\nabla\mathcal{G}_{p_3}(\mathbf{u}^k, s^k, {m_l}^k, {K_l}^k), \qquad {m_l}^{(k+1)} = \mathbf{prox}_{\gamma\mathcal{R}_3}(\overline{m_l}^{(k)}) \tag{3.3}$$

$$\overline{K_l}^{(k)} = {K_l}^k - \gamma\nabla\mathcal{G}_{p_4}(\mathbf{u}^k, s^k, {m_l}^k, {K_l}^k), \qquad {K_l}^{(k+1)} = \mathbf{prox}_{\gamma\mathcal{R}_4}(\overline{K_l}^{(k)}) \tag{3.4}$$

- If $\frac{\|\mathbf{z}^{(k+1)} - \mathbf{z}^{(k)}\|_2}{\|\mathbf{z}^{(k)}\|_2} \le \epsilon$, stop. Otherwise $k = k+1$, go to Step 1.

Remark 3.1. The existence of a Nash equilibrium for the discrete game, i.e., discrete energies, can be handled similarly to the continuous case, i.e., using an inclusion problem and a fixed point methods.

The u-subproblem. Fixing K^k, s^k and m^k and λ_i^k $(i = 1, \dots, 5)$ and using the definition of the proximal operators, the $\mathbf{u}$-subproblem (3.1) amounts to solve

$$\min_{\mathbf{u}}\{\mathcal{R}_1(\mathbf{u}) + \frac{1}{\gamma}\|\mathbf{u} - \overline{\mathbf{u}}^{(k)}\|_2^2\}, \quad \text{w.r.t } \overline{\mathbf{u}}^{(k)} = \mathbf{u}^k - \gamma\nabla\mathcal{G}_{p_1}(\mathbf{u}^k, s^k, {m_l}^k, {K_l}^k),$$

which is equivalent to find the deformation $\mathbf{u} = (u_1, u_2)$ that satisfies the following system of PDEs in Ω:

$$\begin{cases} -\gamma\Delta u_1 + \gamma\mathrm{div}^2[\nabla^2 u_1] + u_1 = u_1^k - \gamma\lambda_1(T(\mathbf{u}^k) - e^{{K_l}^k} - s^k)\partial_x T(\mathbf{u}^k), \\ -\gamma\Delta u_2 + \gamma\mathrm{div}^2[\nabla^2 u_2] + u_2 = u_2^k - \gamma\lambda_1(T(\mathbf{u}^k) - e^{{K_l}^k} - s^k)\partial_y T(\mathbf{u}^k), \end{cases} \tag{3.5}$$

with the periodic boundary conditions on $\partial\Omega$. Here, $\mathbf{u}^k = (u_1^k, u_2^k)$ denotes the solution from the previous iteration for the alternating algorithm. To solve the above fourth-order equations in each iteration, we use the 2-dimensional discrete Fourier transforms. In fact, we have:

$$L_1 \cdot \mathcal{F}(u_1) = \mathcal{F}(F_1(\mathbf{u}^k)), \text{ and } L_1 \cdot \mathcal{F}(u_2) = \mathcal{F}(F_2(\mathbf{u}^k)),$$

where $L = I - \gamma\ \mathcal{F}(\Delta) + \gamma\ \mathcal{F}(\mathrm{div}^2[\nabla^2])$ and

$$F_1(\mathbf{u}^k) = u_1^k - \gamma\lambda_1(T(\mathbf{u}^k) - e^{{K_l}^k} - s^k)\partial_x T(\mathbf{u}^k),$$
$$F_2(\mathbf{u}^k) = u_2^k - \gamma\lambda_1(T(\mathbf{u}^k) - e^{{K_l}^k} - s^k)\partial_y T(\mathbf{u}^k).$$

where I is an $p \times q$ matrix composed of ones, the operator $\mathcal{F}(\cdot)$ is the Fourier transform and "$\cdot$" means point-wise multiplication of matrices. Therefore, the discrete solutions u_1 and u_2 can be obtained by applying the inverse of the discrete two-dimensional Fourier transform to the previous equation and we have:

$$u_1 = \mathcal{F}^{-1}\left(\mathcal{F}(F_1(\mathbf{u}^{old})).\!/L_1\right) \text{ and } u_2 = \mathcal{F}^{-1}\left(\mathcal{F}(F_2(\mathbf{u}^{old})).\!/L_1\right), \tag{3.6}$$

where"$\cdot/$" means the point-wise division.

The s-subproblem. The problem (3.2) is equivalent to solve

$$\min_s\{\mathcal{R}_2(s) + \frac{1}{\gamma}\|s - \overline{s}^{(k)}\|_2^2\}, \text{ w.r.t } \overline{s}^{(k)} = s^k - \gamma\nabla\mathcal{G}_{p_2}(\mathbf{u}^k, s^k, {m_l}^k, {K_l}^k),$$

which leads to its optimality condition:

$$-\gamma\Delta s + s = s^k - \gamma\lambda_2 T(\mathbf{u}^k) - \lambda_2 e^{{K_l}^k} + s^k) \quad \text{or } \hat{L}_1 s = S_2 \tag{3.7}$$

which is a linear problem with the periodic boundary condition on $\partial\Omega$, where we denote

$$\hat{L}_1 = I - \gamma\Delta \quad \textit{and} \quad S_2 =^k -\gamma\lambda_2 T(\mathbf{u}^k) - \lambda_2 e^{{K_l}^k} + s^k).$$

We take advantage of the 2-dimensional discrete Fourier transforms to compute s. In fact, applying the Fourier transforms to discrete forms on both sides of equation (3.7), we get:

$$L_1 \cdot \mathcal{F}(s) = \mathcal{F}(S_2), \quad L = \mathcal{F}(\hat{L}_2) = I - \gamma\mathcal{F}(\Delta),$$

and, therefore, the discrete solution given by:

$$s = \mathcal{F}^{-1}\left(\mathcal{F}(S_2)\cdot/L_1\right), \tag{3.8}$$

where "$\cdot$" means point-wise multiplication of matrices, $\mathcal{F}^{-1}(\cdot)$ is the inverse of the discrete two-dimensional Fourier transform.

The m_l-subproblem. The problem (3.3) leads to the optimality condition:

$$-\gamma\Delta m_l + m_l = {m_l}^k - \gamma(\lambda_3 \ln(T(\mathbf{u}^k) - s^k) - R_l), \tag{3.9}$$

which is a linear problem for m_l. Therefore, the discrete solution is given by:

$$m_l = \mathcal{F}^{-1}\left(\mathcal{F}(S_3)\cdot/L_3\right), \tag{3.10}$$

where $\mathcal{F}^{-1}(\cdot)$ is the inverse of the discrete two-dimensional Fourier transform,

$$L_1 = -\gamma\mathcal{F}(\Delta) + I, \text{ and } S_3 = {m_l}^k - \gamma(\lambda_3 \ln(T(\mathbf{u}^k) - s^k) - R_l).$$

The K_l-subproblem. The problem (3.4) involves computing the proximal operator

$$K_l = \mathbf{prox}_{\gamma\mathcal{R}_4}(\overline{K_l}^{(k)}) = \mathbf{prox}_{\gamma\iota_A} \circ \mathbf{prox}_{\gamma S_4}(\overline{K_l}^{(k)}),$$

where $S_4(K_l) = \int_\Omega |\nabla K_l|^2 \, d\mathbf{x}$. First, we find find the solution $K_l = \mathbf{prox}_{\gamma S_4}(\overline{K_l}^{(k)})$ and which is the unique solution for the linear PDE:

$$-\gamma\Delta K_l + K_l = {K_l}^k - \gamma(\lambda_4({m_l}^k + R_l)) = 0, \tag{3.11}$$

with the periodic boundary condition on $\partial\Omega$. Therefore, the discrete solution is given by

$$K_l = \mathcal{F}^{-1}\left(\mathcal{F}(S_4) \cdot / L_1\right), \quad S_4 = {K_l}^k - \gamma(F'({K_l}^k) + \lambda_4({m_l}^k + R_l)),$$

where $\mathcal{F}^{-1}(\cdot)$ is the inverse of the discrete two-dimensional Fourier transform. After that, we make the projection step $\mathbf{prox}_{\gamma\iota_C}(K_l)$.

Remark 3.2. If periodic boundary conditions cannot be assumed, a fast Fourier transform is not applicable so the four sub-problems have to be solved by other solvers. One good choice would be a linear multigrid solver. Then, the same efficiency can be achieved. We also point out that some images T, R may be padded with zeros at boundaries in order to ensure that zero periodic boundary conditions for $\mathbf{u}$ are reasonable.

4. Numerical results.

In the numerical validation, we assess the performance of the proposed algorithm 3.1 for our new model (denoted by "**New**" below). The experiments will show that the proposed algorithm can have significant robustness in presence of bias noise and varying illumination. In order to balance the energies in our approach, we need an appropriate choice of the weighting parameters. In our tests, we fix the parameters in the model by using $\lambda_1 = 200$ for the $\mathbf{u}$-subproblem, $\lambda_2 = 20$ for the s-subproblem, $\lambda_3 = 1$ for the m_l-subproblem, and $\lambda_4 = 5$ for the K_l-subproblem. These parameters are chosen large enough to satisfy the constraint (1.9). The suitability of these constraints can be seen and checked numerically by the high-similarity between the corrected image T_c and the reference R.

We initialize the displacement $\mathbf{u}$ by a multi-resolution technique, also to avoid local minima and to speed up registration: this is a scale space approach where we resize the original images to a sequence of coarser levels where computations are cheap and register these smaller images. Then starting from the coarsest level, we interpolate the obtained transformation fields to get a starting guess on finer (next) levels until the original resolution on the finest level is reached.

To convince the reader that the new approach is unique and performs better than related and conceivable methods, we include 4 methods on the comparison ist. We denote by "**JM** " the earlier joint model (1.7) where we minimize this global energy directly. This is the model that we must compare with because it is a more natural choice for the class of problems that we study. We also compare the proposed game approach with the non- game approach which consists in solving the classical variational model (1.9) that we denote by "**CV** ". For the numerical implementation of "**JM** " and "**CV** " models, we use an alternating algorithm and iterative procedure [3, 14]. We also compare with the purely multiplicative model proposed in [34] and that we denote by "**MM**".

We also compare with the Mutual Information based multi-modality model where the we minimize an energy which uses $\mathcal{R}_1(\cdot)$ and the Mutual Information as similarity measure (denoted by "**MI**" below). This model is not expected to work well (for this matter nor do all multi-modality models), because a bias field represents redundant or unwanted image features and registering such features rigorously leads to misleading results. In fact, Mutual Information similarity measure fails when features with different intensities in the first image have similar intensities in the second one [30], which is the case in perfusion imaging. Numerical experiments on **MI** are performed using the publicly available image registration toolbox – Flexible algorithms for image registration (FAIR)[1], where the implementation is based on the Gauss-Newton method.

As a final comparison, we also present results from a two-stage approach (named as "**TS**"): In stage 1, we use the correction model (1.5), where for to choose the regularizer $\mathcal{R}(\cdot)$, we borrow the idea from model (1.4) and we consider:

$$\mathcal{R}(T^*, m, s) = \nu_1 \int_\Omega |\nabla^2 m|^2 d\mathbf{x} + \nu_2 \int_\Omega |\nabla^2 s|^2 d\mathbf{x} + \kappa \int_\Omega |T^*|^2 d\mathbf{x} + \mu \int_\Omega \Phi_\epsilon(|DT^*|) d\mathbf{x}.$$

For the numerical resolution of Step 1, we use an alternating algorithm similar to Algorithm (3.1). In Stage 2, we minimize an energy (1.6) where $\mathcal{R}_1(\cdot)$ is the regularizer and the sum of squared difference (SSD) is the similarity measure between the estimated image T^* which will be moved and the reference R, i. e., $\|T^*(\mathbf{u}) - R\|_2^2$. This approach is also natural and in fact there exist many works that aim to correct bias fields. We do not expect that such a two-stage idea works well because (as remarked before) removing bias from a single image is insufficient due to lack of guide of a second image to differentiate valid features and bias regions without user input.

We note that the corrected and registered image is $T_c(\mathbf{u})$, not $T(\mathbf{u})$ which registers to $mR + s$, as respectively defined by the formula $T_c = (T(\mathbf{u}) - s)/e^{m_l}$ for "**New**" and "**CV** ", and $T_c = (T(\mathbf{u}) - s)/m$ for "**JM**" and "**TS**" (as discussed in (1.3)). In contrast, the final registered image for "**MI**" is just $T(\mathbf{u})$. We also use the normalized correlation coefficient (NCC) between T_c and R to quantify the performance of the models and the comparison (the closer the NCC is to 1, the better is the alignment). For **MI model**, NCC between $T(\mathbf{u})$ and R also makes sense.

Test example 1. We start our numerical validation on a pair of synthetic images. In Fig 1, we consider an image of a disk as reference and a bigger disk with a grayscale rectangle on its interior as template. We compare **New**, **JM** and **MM**. For each model, we plot the registered image $T(\mathbf{u})$, the corrected image $T_c(\mathbf{u})$, and the difference (error) between them. The registered image obtained using **New** is clearly better than the ones obtained using **JM** and **MM**. In Fig. 2, we also display the corrected images and the auxiliary the variables involved in all compared models. The corrected image using **New** seems to be very close to the reference and it is better than the result obtained using **New** and **MM**. Moreover, **New** performs better than **JM** and **MM** registration as well as in intensity correction. We have added colorbars to the figures. The colorbars show that **New** and **MM** models give

[1]http://www.siam.org/books/fa06/

comparable results in intensity correction, with both performing better than **JM** model. However, in registration, **New** model is better than the other competitive models **MM** and **JM**. We also show the resulting transformed grids for all models where there is no mesh folding.

Test example 2: MRI images. In Fig. 3, we register two MRI images and display the transformed images $T(\mathbf{u})$ using all tested models where the moving image T (synthetically enhanced) contains some bias field and varying illumination. In Fig. 4, we plot the variables s, m_l and the corrected image $T_c(\mathbf{u})$ using **New**, **CV**, **JM** and **TS model**. We see that all models except **MI model** perform well in most parts of the image, but in the middle of the images our **New** is the most advantageous and we can observe the zoomed details in Fig. 5. We can see visually a big difference in the recovered m and s because these quantities are not estimated from the same images. In fact, m and s are estimated from the initial image T in the first step of **TS** model where no information from R is used; in contrast, the other models estimate m and s using both T and R.

We also compute the determinant of the Jacobians and find that there is no mesh folding in all cases i.e. the transformations are physically plausible. In other tests, we tabulate the run times for the different models and in different resolutions in Table 1. As seen, these are comparable. For the parameters tuning, we have added Table 2 to indicate the registration results for different parameters λ_i $(i = 1, ..., 4)$. The table shows that the game approach is stable.

In Fig. 8, we plot the relative residual errors for **New**, and **JM** for all variables as functions of iterations in **Algorithm 1**. For **New**, the errors of the three variables decrease very well for all variables in the same time, which explains the ability of this model to handle all the objectives jointly. However, the errors for the **JM** decrease slowly for all variables except the for the displacement $\mathbf{u}$, where a convergence problem is clearly seen. This behaviour make clear the inability of **JM** in handling all objectives jointly, i. e., non-accurate in the registration task We also plot the curve representing the energies $E_r = \|T(\mathbf{u}) - \exp^{R_l} \exp^{m_l} - s\|$ for **New** and $E_r = \|T(\mathbf{u}) - mR - S\|$ for **JM**.

For the same pair of images, we consider the additive and multiplicative cases (not combined bias) separately:
(1) First in Fig. 6, the template image T has additive bias field only. We give the results of the all compared models. The results show that **New** model outperforms the competitive models and gives better results mainly for registration. For the intensity correction task, all models give similar results.
(2) Second in Fig. 7, the template image T has multiplicative bias field only. Again we compare 4 models as before and we see that **New** model either outperforms or performs equally well.

The results underline the good performance of **New** model in solving both problems effectively.

Test example 3: Application to Perfusion CT registration. In Fig. 10, we consider a pair of CT and Perfusion CT lung images. As we can see in the middle of the images images T and R, there is a big difference because the high contrast in T and which makes inefficient the use of classical mono-modal measures. We show the registered images using **New**, **CV**, **JM**,

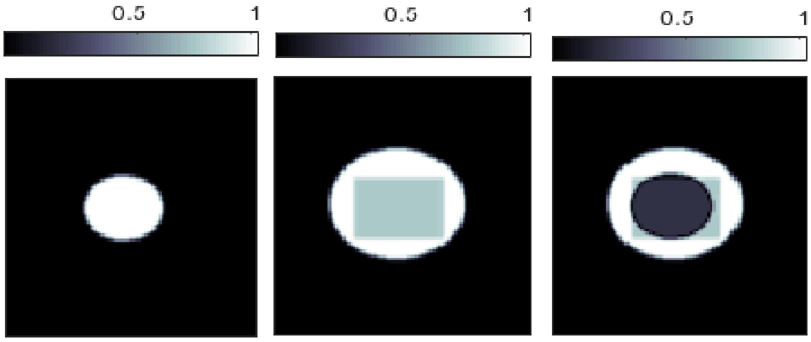

(a) The reference R (b) The template T (c) The difference $|T-R|$

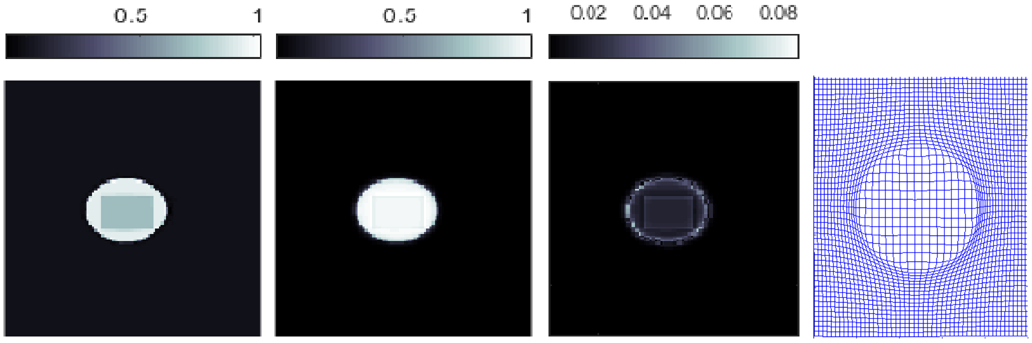

(d) **New**: $T(\mathbf{u})$ only (e) **New** $T_c(\mathbf{u})$, NCC=0.99 (f) **New**: $|T_c(\mathbf{u}) - R|$ (g) **New**: The grid

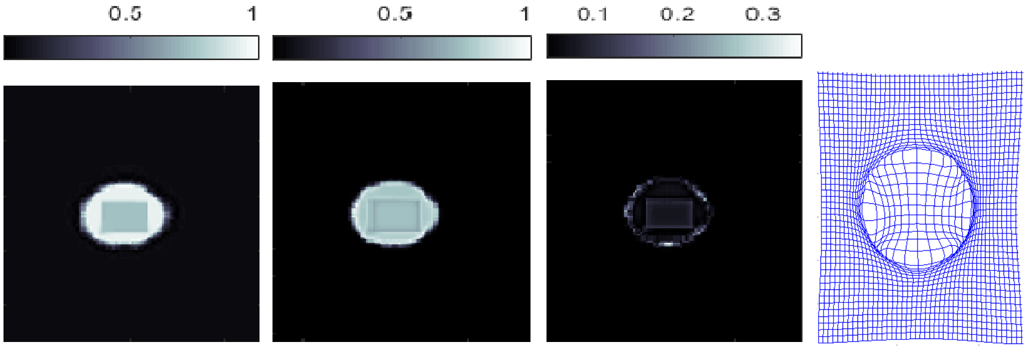

(h) **JM** : $T(\mathbf{u})$ only (i) **JM**: $T_c(\mathbf{u})$, NCC=0.98 (j) **JM**: $|T_c(\mathbf{u}) - R|$ (k) : The grid

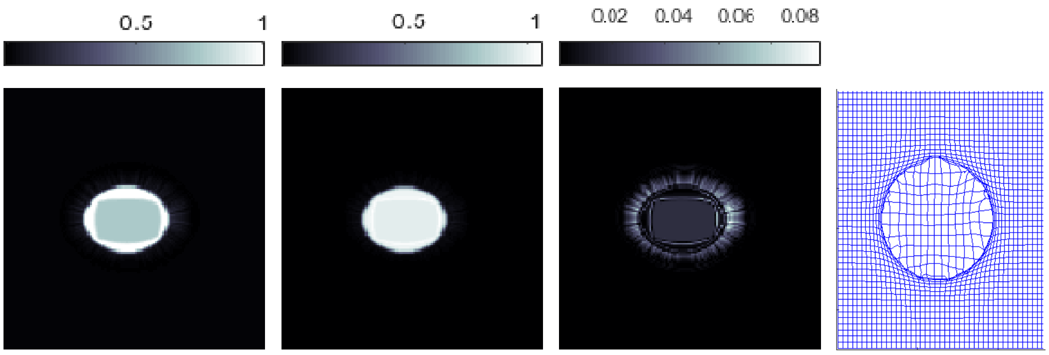

(l) **MM**: $T(\mathbf{u})$ only (m) **MM**: $T_c(\mathbf{u})$, NCC=0.98 (n) **MM**: $|T_c(\mathbf{u}) - R|$ (o) **MM**: The grid

Figure 1. *Example 1: Comparison between* **New**, **JM** *and* **MM** *for registering a pair of synthetic images. Here in both cases, displaying $T(\mathbf{u})$ is for information only and we do not show the big difference $|T(\mathbf{u}) - R|$ for the intermediate and uncorrected quantity $T(\mathbf{u})$ which registers to $mR + s$, not to R – see (1.3).*

(2019)

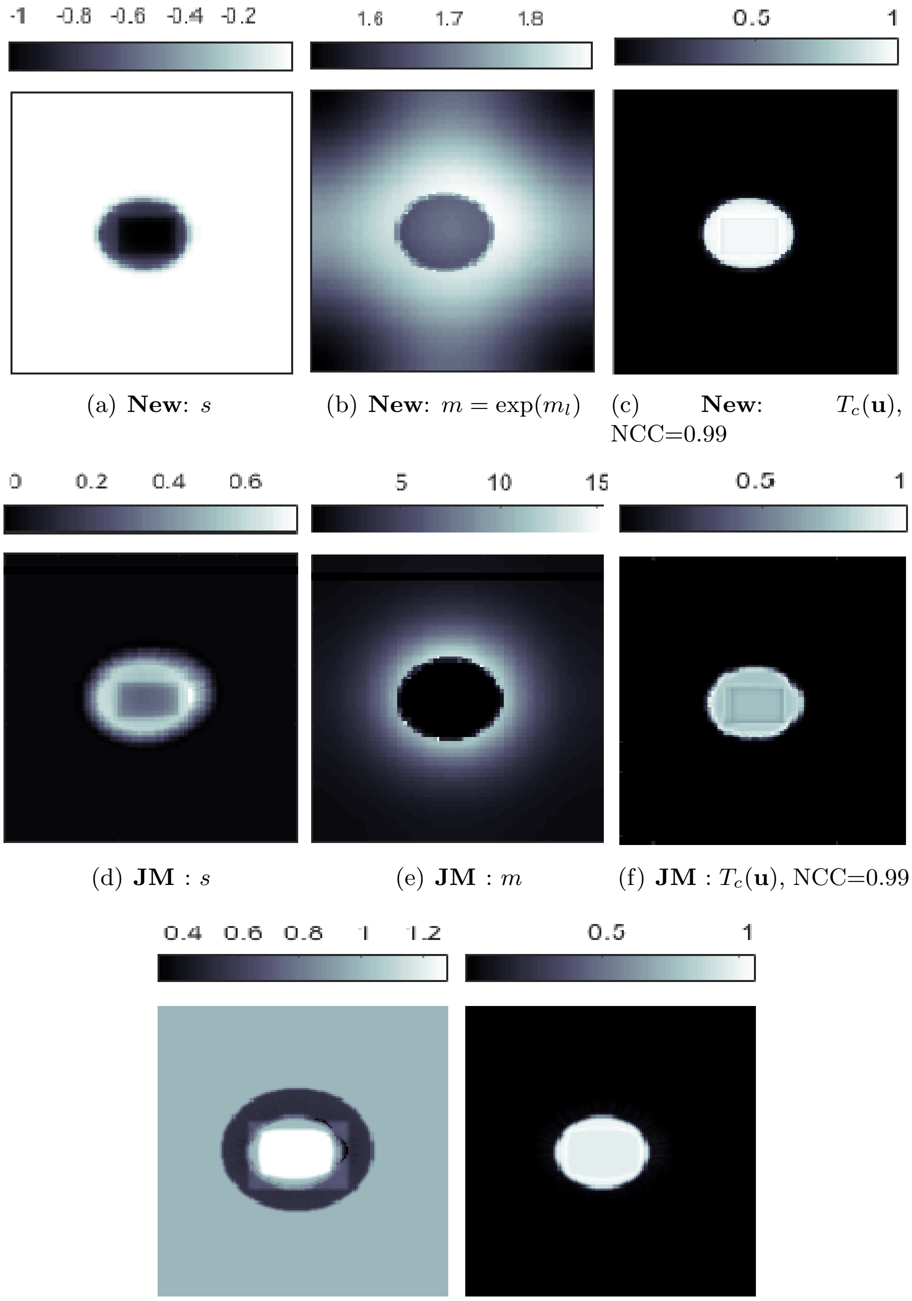

(a) **New**: s (b) **New**: $m = \exp(m_l)$ (c) **New**: $T_c(\mathbf{u})$, NCC=0.99

(d) **JM** : s (e) **JM** : m (f) **JM** : $T_c(\mathbf{u})$, NCC=0.99

(g) **MM**: m (h) **MM**: $T_c(\mathbf{u})$, NCC=0.98

Figure 2. *Example 1 – The variables s, $m = \exp(m_l)$ and $T_c(\mathbf{u})$ obtained using —**New**, the variables s, m and $T_c(\mathbf{u})$ obtained using —**JM** and the the variables m and $T_c(\mathbf{u})$ obtained using —**MM**.*

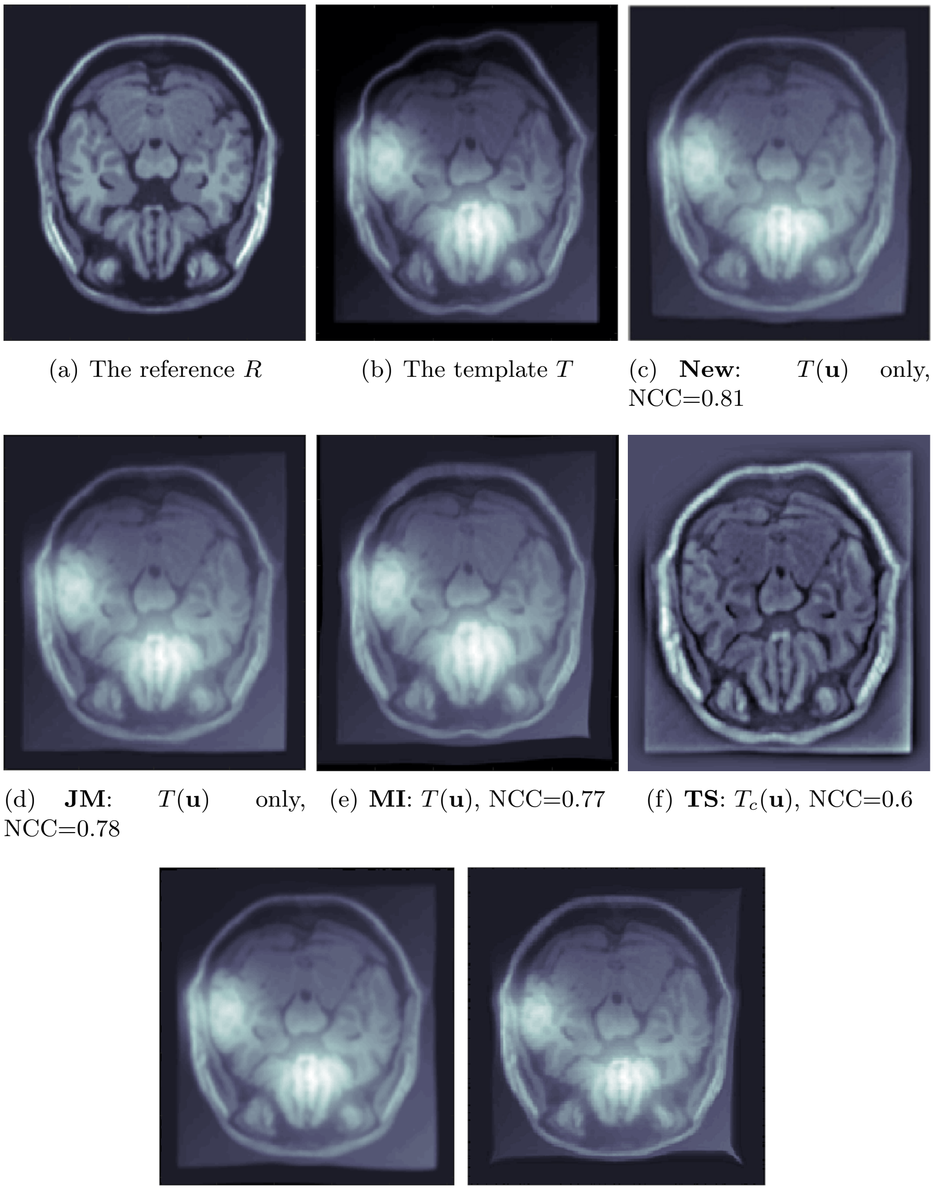

(a) The reference R (b) The template T (c) **New**: $T(\mathbf{u})$ only, NCC=0.81

(d) **JM**: $T(\mathbf{u})$ only, NCC=0.78 (e) **MI**: $T(\mathbf{u})$, NCC=0.77 (f) **TS**: $T_c(\mathbf{u})$, NCC=0.6

(g) **CV**: $T_c(\mathbf{u})$, NCC=0.79 (h) **MM**: $T_c(\mathbf{u})$, NCC=0.79

Figure 3. *Example 2: Comparison of* 5 *different models to register MRI T-1 and T-2 images. From this figure and Figs.5-4, we see that* **New** *gives the best registration result.*

TS model, **MM** and **MI model**. The main dissimilarity between all models is highlighted by zooming in the middle parts of the images in Fig. 12. We easy see that **New** gives a satisfactory result and the corrected part of the moving image is very similar to the middle part of the reference whereas the registration is not good. For New model, the result of both registration and correction is satisfactory and this underlines the performance of this model

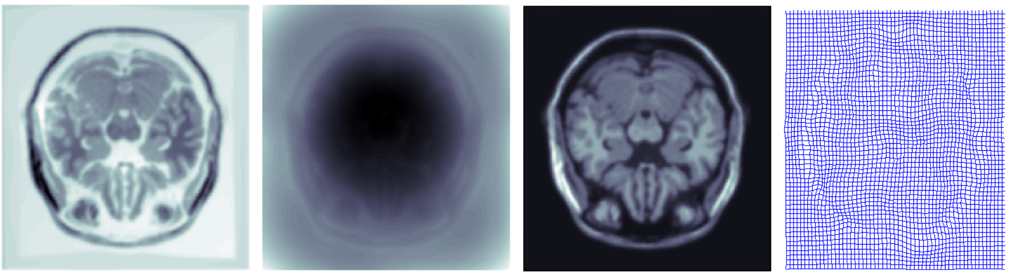

(a) **New**: s (b) **New**: $m = \exp(m_l)$ (c) **New** $T_c(\mathbf{u})$ NCC=0.99 (d) **New**: The grid

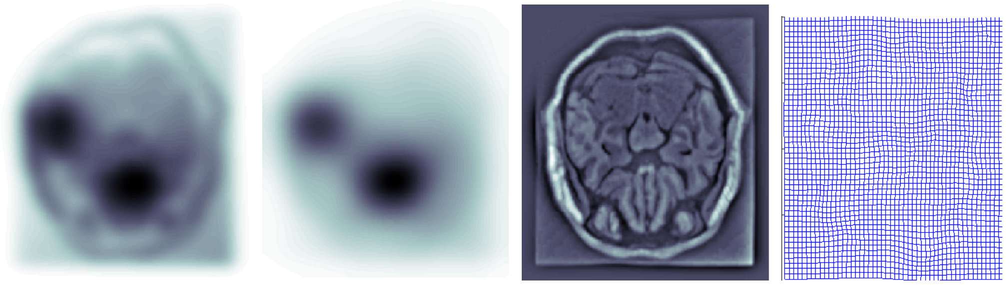

(e) **TS**: s from Step 1 (f) **TS**: Step 1 m (g) **TS**: $T_c(\mathbf{u})$ NCC=0.6 (h) **TS**: The grid

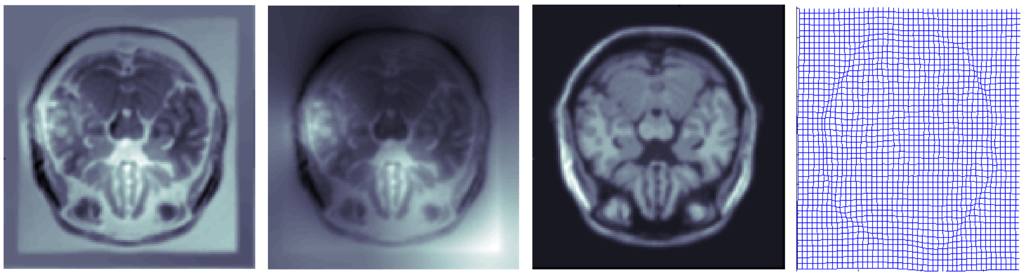

(i) **JM** : s (j) **JM**: m (k) **JM**: $T_c(\mathbf{u})$, NCC=0.98 (l) **JM**: The grid

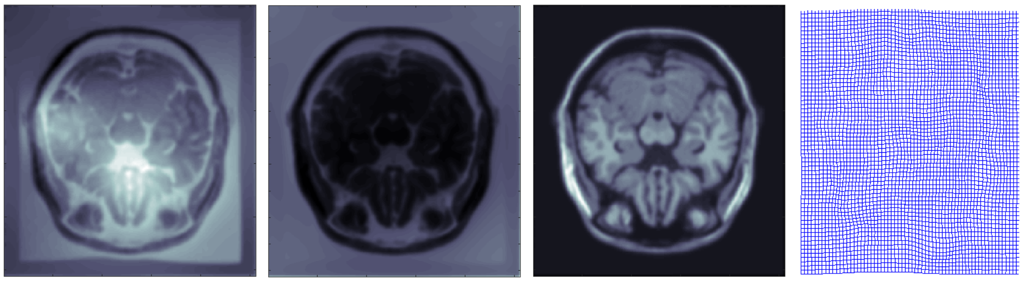

(m) **CV**: s (n) **CV**: $m = \exp(m_l)$ (o) **CV** $T_c(\mathbf{u})$ NCC=0.99 (p) **CV**: The grid

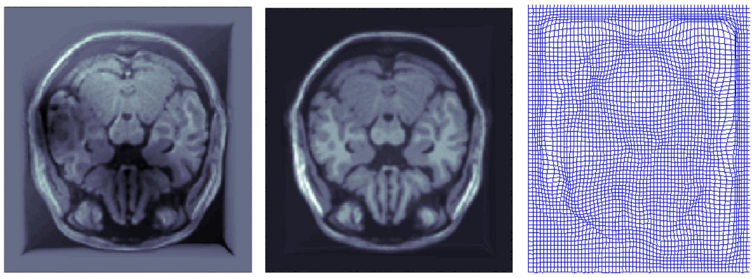

(q) **MM**: m (r) **MM**: $T_c(\mathbf{u})$ NCC=0.97 (s) **MM**: The grid

(2019)

Figure 4. *Example 2 – Comparison of* **New**, **JM**, **TS** *and* **MM** *in intensity correction*

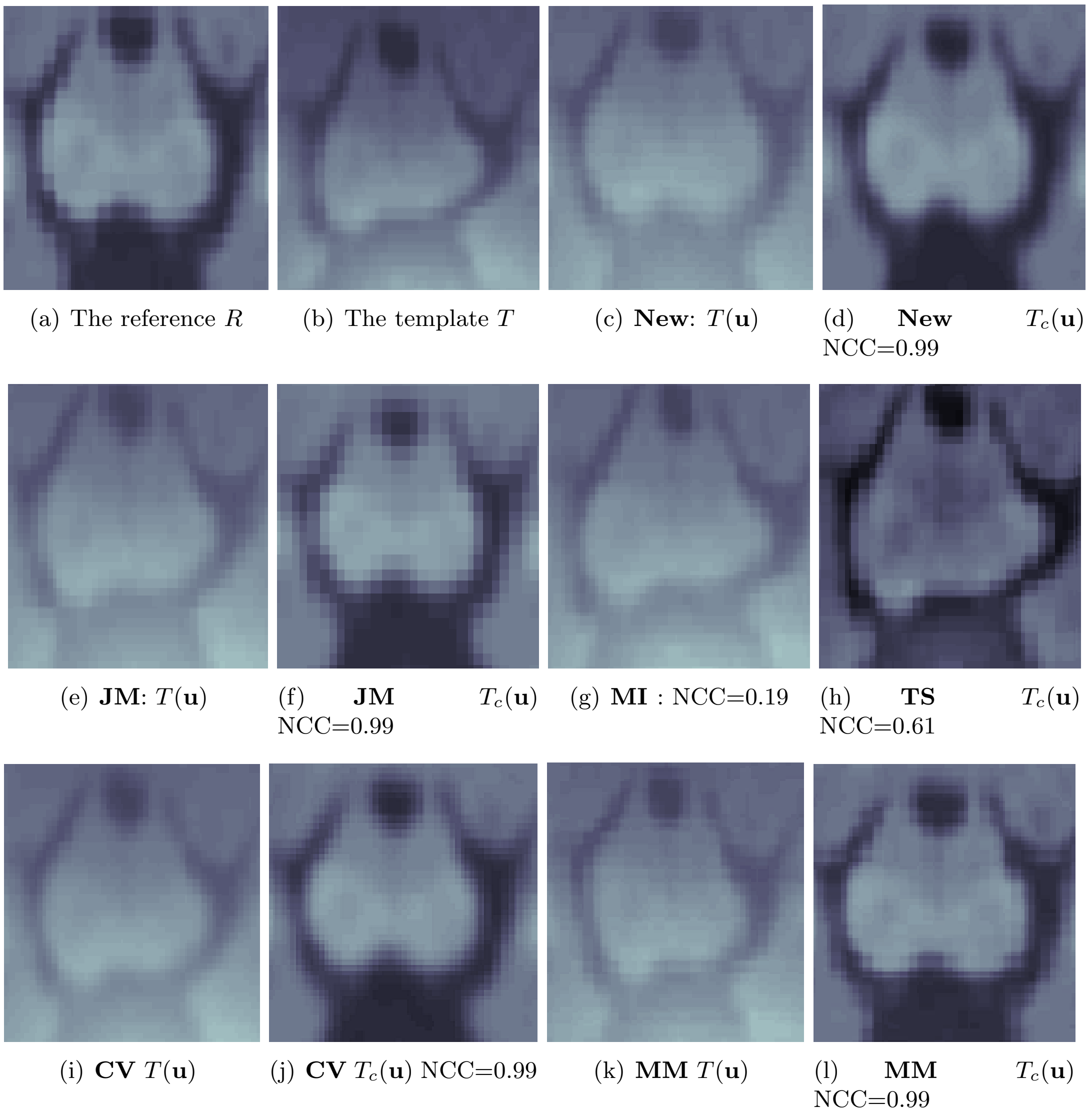

(a) The reference R (b) The template T (c) **New**: $T(\mathbf{u})$ (d) **New** $T_c(\mathbf{u})$ NCC=0.99

(e) **JM**: $T(\mathbf{u})$ (f) **JM** $T_c(\mathbf{u})$ NCC=0.99 (g) **MI** : NCC=0.19 (h) **TS** $T_c(\mathbf{u})$ NCC=0.61

(i) **CV** $T(\mathbf{u})$ (j) **CV** $T_c(\mathbf{u})$ NCC=0.99 (k) **MM** $T(\mathbf{u})$ (l) **MM** $T_c(\mathbf{u})$ NCC=0.99

Figure 5. *Example 2: Compared zoom regions of* 5 *different models to register MRI T-1 and T-2 images. Again* **New** *is the best in solving the registration and the intensity correction jointly, whereas* **JM** *and* **MM** *cannot solve both problem jointly, only the image correction task is successful.*

in solving both problems jointly and efficiently which is not the case for **CV**, **JM** and **MI** and **MM** as they only handle the correction task correctly and fail in registration. For this particular example, $T(\mathbf{u})$ is very useful as clinicians like to where the contrasts from perfusion CT ('artefacts') would be located on the CT.

Test example 4: Generalisation to three dimensional formulation. The work presented so far can be generalized to register images in three dimensions (3D). For a 3D registration problem, we have $\Omega \subset \mathbb{R}^3$ and $\mathbf{u} = (u_1, u_2, u_3)$. The four energy functionals in (2.2) still take

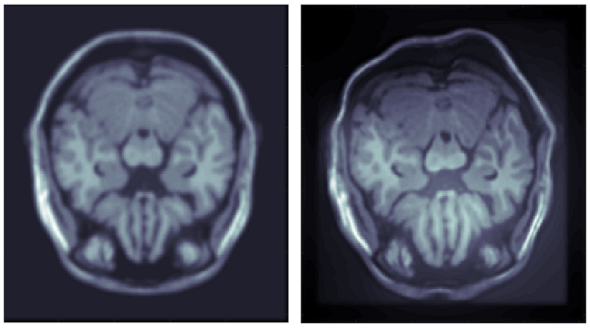

(a) The reference R (b) The template T

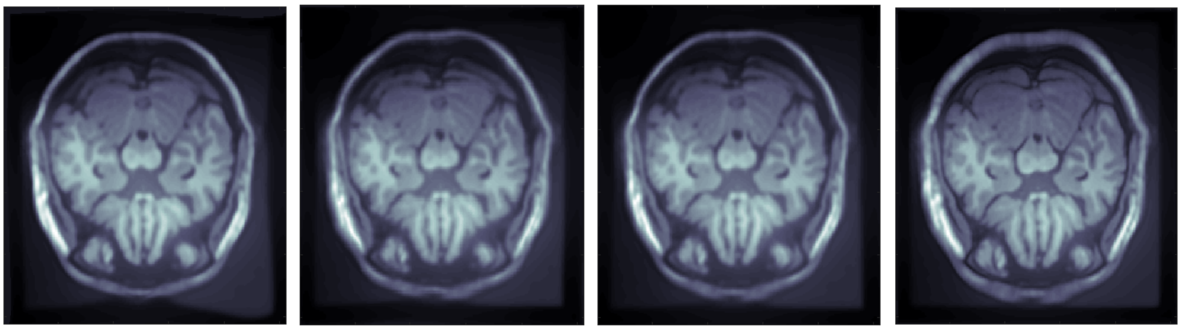

(c) **New**: $T(\mathbf{u})$ only, NCC=0.92 (d) **CV**: $T(\mathbf{u})$ only, NCC=0.91 (e) **JM**: $T(\mathbf{u})$ only, NCC=0.91 (f) **MM**: $T(\mathbf{u})$ only, NCC=0.9

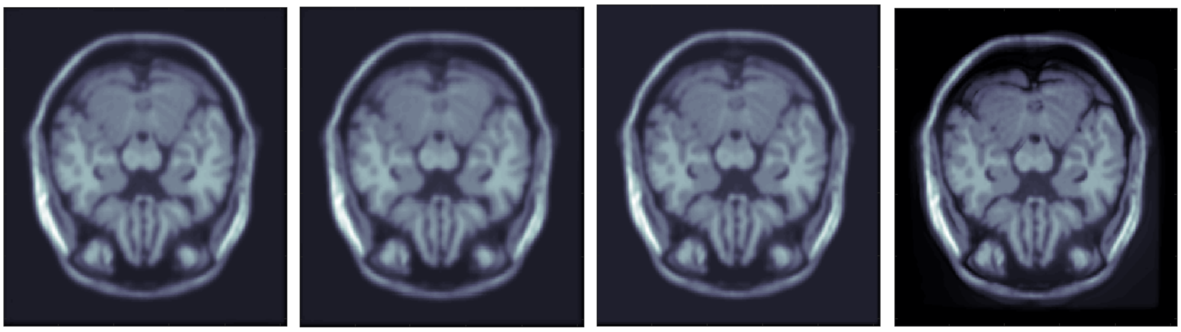

(g) **New**: $T_c(\mathbf{u})$, NCC=0.99 (h) **CV**: $T_c(\mathbf{u})$, NCC=0.99 (i) **JM**: $T_c(\mathbf{u})$, NCC=0.99 (j) **MM**: $T_c(\mathbf{u})$, NCC=0.97

Figure 6. *Comparison of* 4 *different models to register MRI T-1 and T-2 images for only additive intensity correction. From this figure, we see that* **New** *gives the best registration result.*

the same forms and we apply **Algorithm 3.1**. Similar to the 2D case, a 3D multi-resolution technique is used as well in order to avoid local minima and to speed up registration.

To demonstrate this generalization, in Fig. 13, we display the result of registering 3D CT and Perfusion CT images where the reference R and the template T have the same size of $512 \times 512 \times 16$. The perfusion images contain highly contrasted regions mainly in the middle of the images. This high contrast plays the same role of bias field (as in 2D) so we expect that

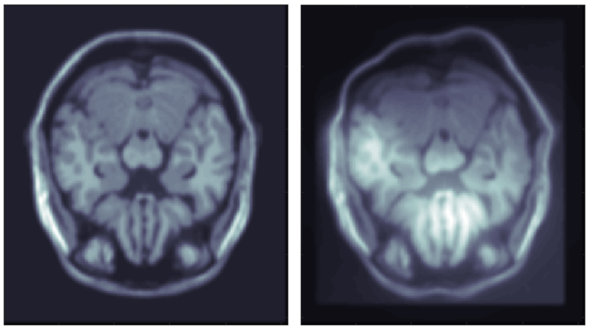

(a) The reference R (b) The template T

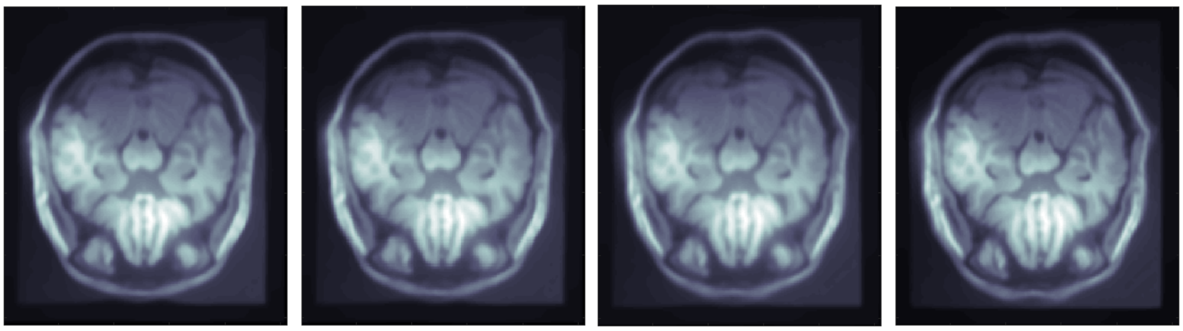

(c) **New**: $T(\mathbf{u})$ only, NCC=0.88 (d) **CV**: $T(\mathbf{u})$ only, NCC=0.87 (e) **JM** : $T(\mathbf{u})$ only, NCC=0.86 (f) **MM**: $T(\mathbf{u})$ only, NCC=0.84

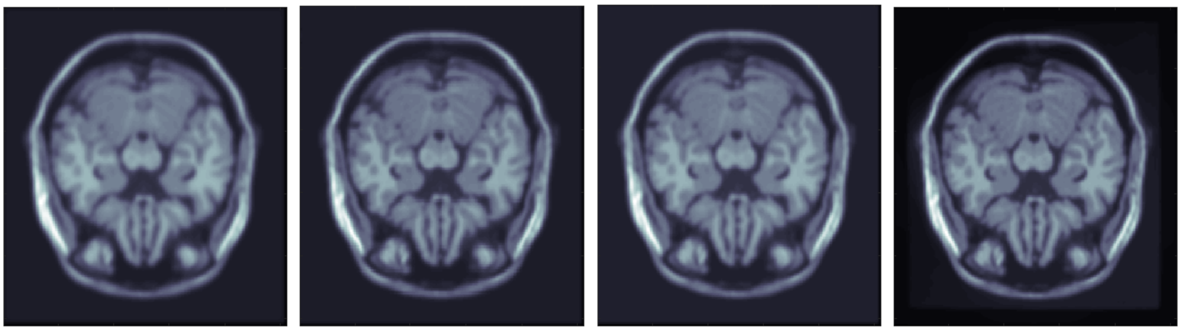

(g) **New**: $T_c(\mathbf{u})$, NCC=0.99 (h) **CV**: $T_c(\mathbf{u})$, NCC=0.99 (i) **JM**: $T_c(\mathbf{u})$, NCC=0.99 (j) **MM**: $T_c(\mathbf{u})$, NCC=0.99

Figure 7. *Comparison of* 4 *different models to register MRI T-1 and T-2 images for only multiplicative intensity correction. From this figure, we see that* **New** *gives the best registration result.*

New is suitable for this case. We display the multiple image frames as rectangular montage. We see that the images are well aligned from the set of the difference images before and after registration.

5. Conclusions.

Image registration is a challenging modelling task with a broad range of applications, in particular in medical imaging. The work presented in this paper deals

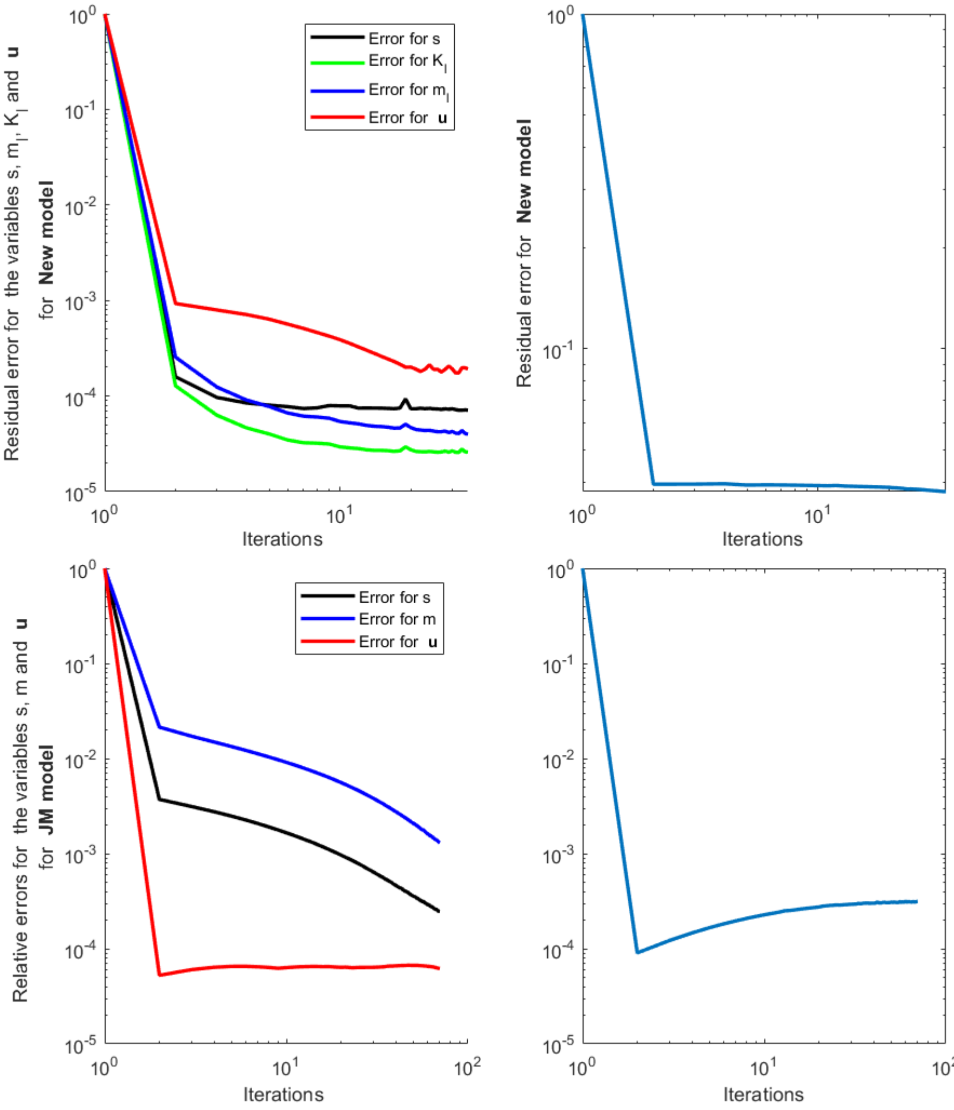

Figure 8. *Display of relative errors (left) and the Fitting energies (right) for the* **New** *and* **JM**. *Evidently the curve of the displacement* **u** *for* **JM** *does not decrease which could explain the non-accuracy in the registration task.*

with the problem of image registration under varying illumination and translation, which can be common in real life cases, such that MRI images. This work is beyond both single-modality and multi-modality image registration models, since a correction step is necessary but yet cannot be done separately. We analysed the proposed model and its the numerical algorithm employed. Numerical realisations have shown the proposed method out-performs the compared classical approaches.

REFERENCES

(2019)

	Resolution			
	64×64	128×128	256×256	512×512
Time (s) for **New**	8.28	17.30	41.04	62.65
Time (s) for **JM**	6.49	14.82	37.13	57.42
Time (s) for **MI**	5.19	10.7	30.70	44.46
Time (s) for **MM**	5.67	13.11	34.54	49.59
Time (s) for **CV**	8.32	17.23	42.12	60.15

Table 1

Run time comparison for all models for the pair of MRI images in Fig.3.

Parameters			
λ_1	λ_2 | NCC	λ_3 | NCC	λ_4 | NCC
100	05 |NCC=0.77	0.5 |NCC=0.78	01 |NCC=0.78
150	15 |NCC=0.79	01 |NCC=0.80	05 |NCC=0.80
200	20 |NCC=0.80	05 |NCC=0.80	20 |NCC=0.79
250	40 |NCC=0.79	10 |NCC=0.77	50 |NCC=0.78
	$\lambda_3 = 1$ and $\lambda_4 = 5$	$\lambda_2 = 20$ and $\lambda_4 = 5$	$\lambda_2 = 20$ and $\lambda_3 = 1$

Table 2

Parameters tuning for the pair of MRI images in Fig.3 using **New** *model. In the first column, we fix the parameters λ_3 and λ_4 and we vary the parameters λ_1 and λ_2. In the third column, we vary λ_1 and λ_3 where λ_2 and λ_4 are fixed, whereas, in the last column, we vary λ_1 and $\lambda_3 4$ for fixed λ_2 and λ_3. The NCC errors for the different values of parameters are comparable.*

[1] K. Aghajani, M. T. Manzuri, and R. Yousefpour, *A robust image registration method based on total variation regularization under complex illumination changes*, Computer methods and programs in biomedicine, 134 (2016), pp. 89–107.

[2] H. Attouch, J. Bolte, P. Redont, and A. Soubeyran, *Alternating proximal algorithms for weakly coupled convex minimization problems. applications to dynamical games and pde's*, Journal of Convex Analysis, 15 (2008), p. 485.

[3] H. Attouch, L. M. Briceno-Arias, and P. L. Combettes, *A parallel splitting method for coupled monotone inclusions*, SIAM Journal on Control and Optimization, 48 (2010), pp. 3246–3270.

[4] H. Attouch and M. Soueycatt, *Augmented lagrangian and proximal alternating direction methods of multipliers in hilbert spaces. applications to games, pde's and control*, Pacific Journal of Optimization, 5 (2008), pp. 17–37.

[5] R. Bansal, L. H. Staib, and B. S. Peterson, *Correcting nonuniformities in mri intensities using entropy minimization based on an elastic model*, in International conference on medical image computing and computer-assisted intervention, Springer, 2004, pp. 78–86.

[6] J.-F. Bonnans, J. C. Gilbert, C. Lemaréchal, and C. A. Sagastizábal, *Numerical optimization: theoretical and practical aspects*, Springer Science & Business Media, 2006.

[7] S. Boyd, N. Parikh, E. Chu, B. Peleato, J. Eckstein, et al., *Distributed optimization and statistical learning via the alternating direction method of multipliers*, Foundations and Trends® in Machine learning, 3 (2011), pp. 1–122.

[8] L. M. Briceno-Arias and P. L. Combettes, *Monotone operator methods for nash equilibria in non-potential games*, in Computational and Analytical Mathematics, Springer, 2013, pp. 143–159.

[9] M. Burger, J. Modersitzki, and L. Ruthotto, *A hyperelastic regularization energy for image registration*, SIAM Journal on Scientific Computing, 35 (2013), pp. 132–148.

[10] H. Chang, W. Huang, C. Wu, S. Huang, C. Guan, S. Sekar, K. K. Bhakoo, and Y. Duan, *A new variational method for bias correction and its applications to rodent brain extraction*, IEEE

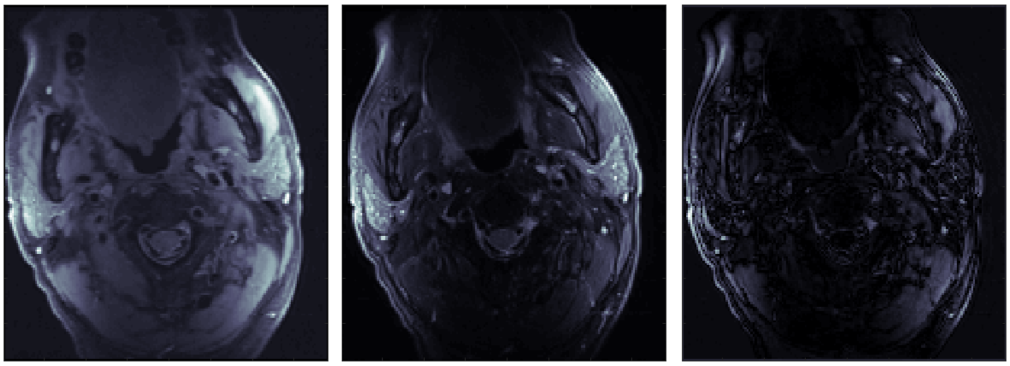

(a) The reference R (b) The template T (c) The difference $|T - R|$

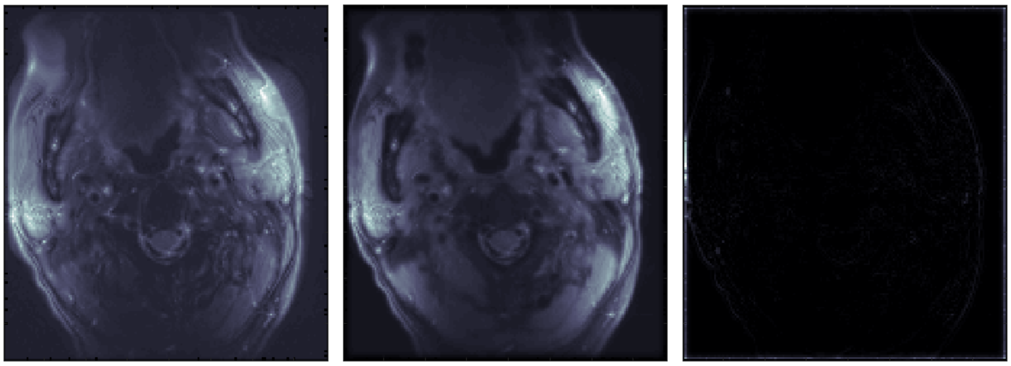

(d) **New**: $T(\mathbf{u})$ only, NCC=0.75 (e) **New**: $T_c(\mathbf{u})$ NCC=0.89 (f) **New**: $|T_c(\mathbf{u}) - R|$

Figure 9. *Example 3: Registration of T1 and T2-MRI images by* **New**

transactions on medical imaging, 36 (2017), pp. 721–733.

[11] N. Chumchob, *Vectorial total variation-based regularization for variational image registration*, IEEE Transactions on Image Processing, 22 (2013), pp. 4551–4559.

[12] N. Chumchob and K. Chen, *Improved variational image registration model and a fast algorithm for its numerical approximation*, Numerical Methods for Partial Differential Equations, 28 (2012), pp. 1966–1995.

[13] N. Chumchob, K. Chen, and C. Brito-Loeza, *A fourth-order variational image registration model and its fast multigrid algorithm*, Multiscale Modeling & Simulation, 9 (2011), pp. 89–128.

[14] P. L. Combettes, *Solving monotone inclusions via compositions of nonexpansive averaged operators*, Optimization, 53 (2004), pp. 475–504.

[15] M. Droske and W. Ring, *A mumford–shah level-set approach for geometric image registration*, SIAM journal on Applied Mathematics, 66 (2006), pp. 2127–2148.

[16] Y. Duan, H. Chang, W. Huang, J. Zhou, Z. Lu, and C. Wu, *The l_{0} regularized mumford–shah model for bias correction and segmentation of medical images*, IEEE Transactions on Image Processing, 24 (2015), pp. 3927–3938.

[17] L. C. Evans, *Partial Differential Equations*, vol. 19 of Graduate Studies in Mathematics, American Mathematical Society, Providence, Rhode Island, 1998.

[18] B. Fischer and J. Modersitzki, *Fast diffusion registration*, Contemp. Math., 313 (2002), pp. 117–129.

[19] B. Fischer and J. Modersitzki, *Curvature based image registration*, Journal of Mathematical Imaging and Vision, 18 (2003), pp. 81–85.

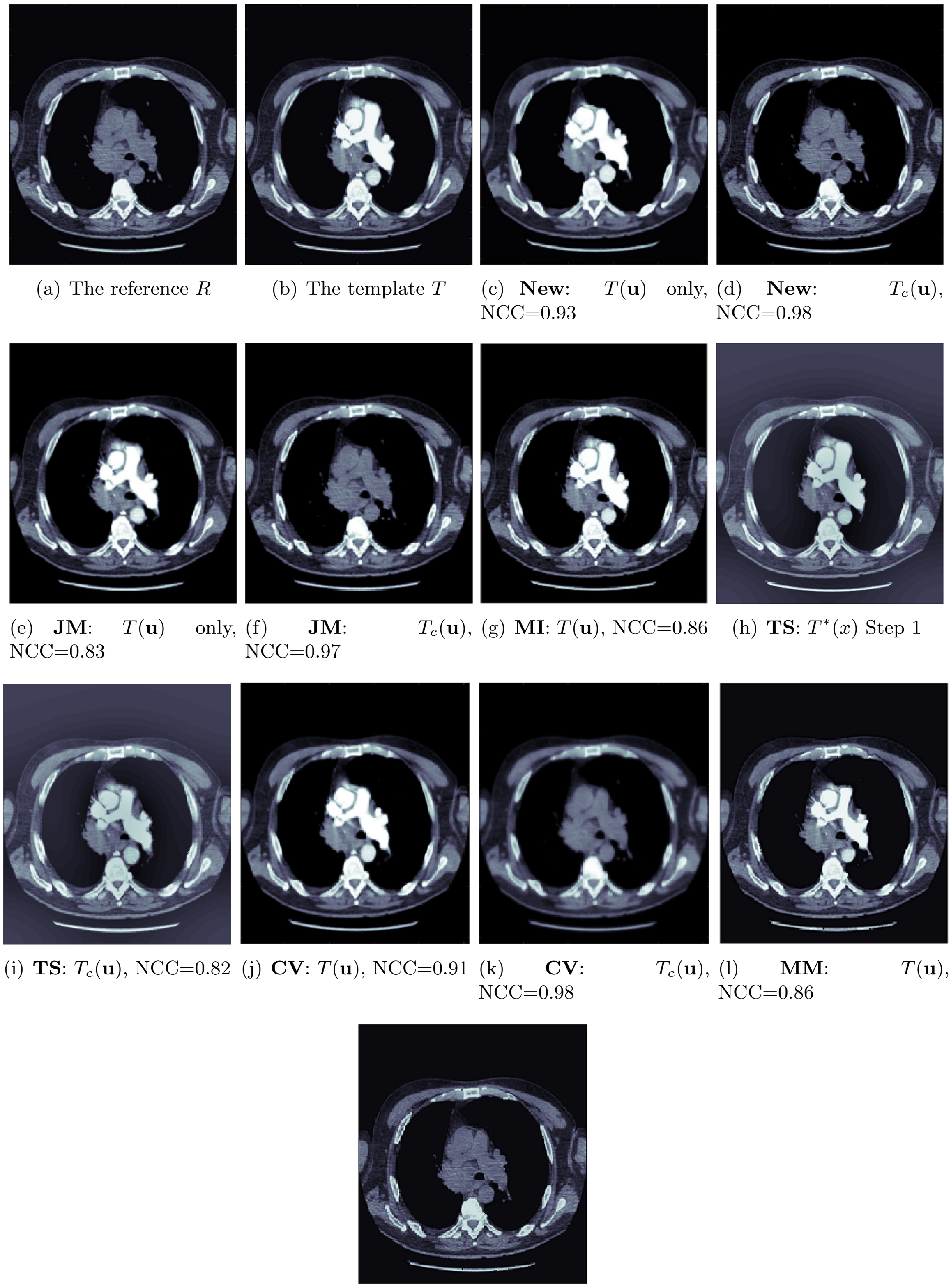

(a) The reference R

(b) The template T

(c) **New**: $T(\mathbf{u})$ only, NCC=0.93

(d) **New**: $T_c(\mathbf{u})$, NCC=0.98

(e) **JM**: $T(\mathbf{u})$ only, NCC=0.83

(f) **JM**: $T_c(\mathbf{u})$, NCC=0.97

(g) **MI**: $T(\mathbf{u})$, NCC=0.86

(h) **TS**: $T^*(x)$ Step 1

(i) **TS**: $T_c(\mathbf{u})$, NCC=0.82

(j) **CV**: $T(\mathbf{u})$, NCC=0.91

(k) **CV**: $T_c(\mathbf{u})$, NCC=0.98

(l) **MM**: $T(\mathbf{u})$, NCC=0.86

(m) **MM**: $T_c(\mathbf{u})$, NCC=0.97

Figure 10. *Example 4: Comparison of* 5 *different models in registering CT and perfusion CT images.* **New** *performs the best.*

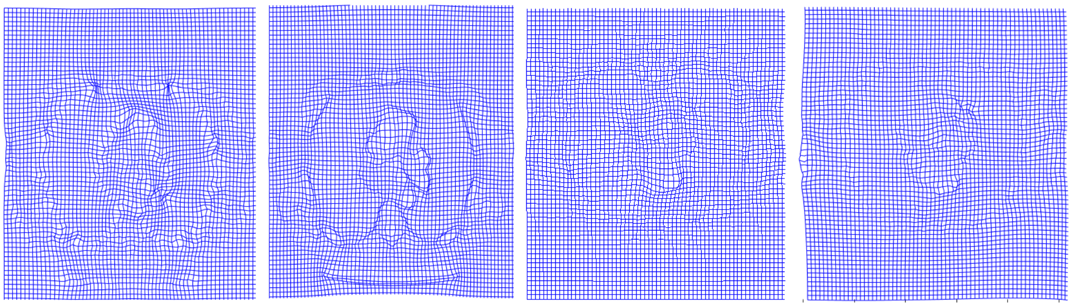

(a) **New** (b) **JM** (c) **TS** (d) **MM**

Figure 11. *Example 4 – The deformed girds using* **New**, **JM**, **TS** *and* **MM** *models*

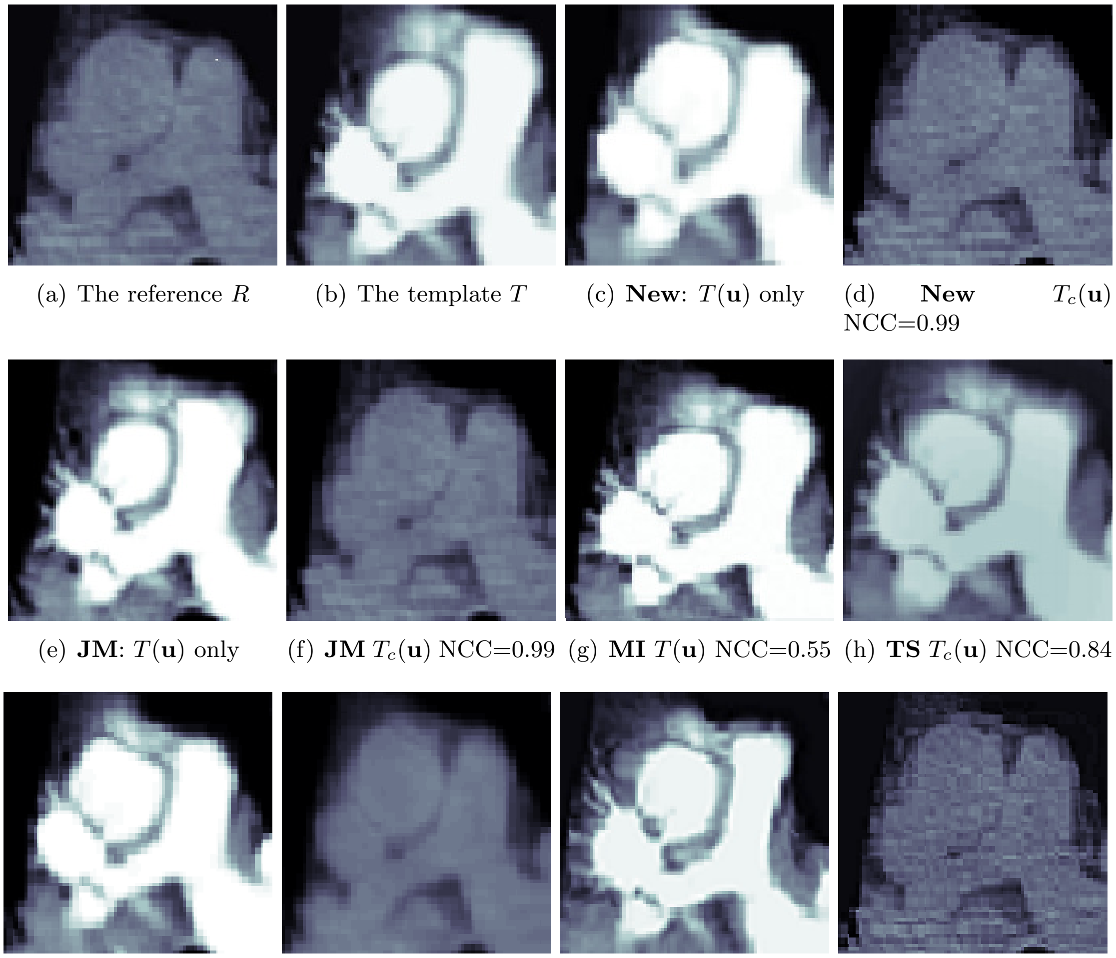

(a) The reference R (b) The template T (c) **New**: $T(\mathbf{u})$ only (d) **New** $T_c(\mathbf{u})$ NCC=0.99

(e) **JM**: $T(\mathbf{u})$ only (f) **JM** $T_c(\mathbf{u})$ NCC=0.99 (g) **MI** $T(\mathbf{u})$ NCC=0.55 (h) **TS** $T_c(\mathbf{u})$ NCC=0.84

(i) **CV** $T(\mathbf{u})$ (j) **CV** $T_c(\mathbf{u})$ NCC=0.98 (k) **MM** $T(\mathbf{u})$ NCC=0.55 (l) **MM** $T_c(\mathbf{u})$ NCC=0.98

Figure 12. *Example 4 zoomed in: Comparison of* 4 *different models to register CT and perfusion CT images. Again* **New** *is the best in obtaining both registration and intensity correction.*

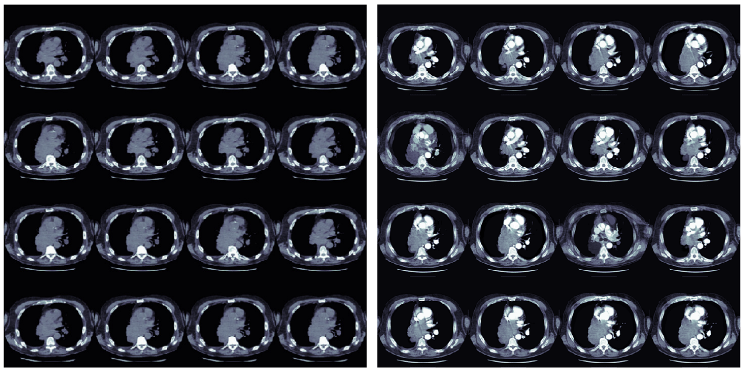

(a) Set of reference images R (b) Set of template images T

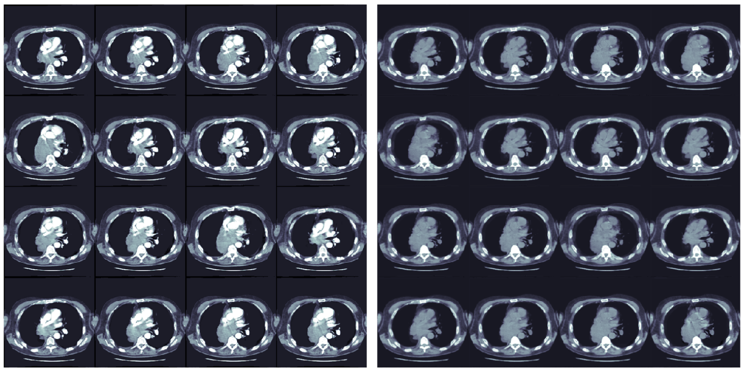

(c) **New**: set of aligned images $T(\mathbf{u})$ only (d) **New**: set of corrected images $T_c(\mathbf{u})$, NCC=0.98

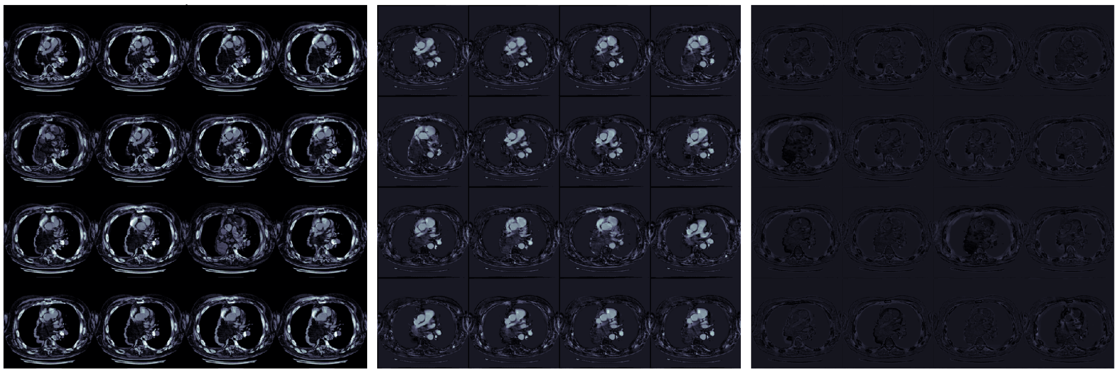

(e) Set of the difference images $|T - R|$ before registration (f) **New**: set of the difference images $|T(\mathbf{u}) - R|$ (g) **New**: set of the difference images $|T_c(\mathbf{u}) - R|$ after registration

Figure 13. *Example 5: Registration of 3D CT and Perfusion CT images of size* $512 \times 512 \times 16$. *Note* $T(\mathbf{u}) \approx mR+s$ *so* $T(\mathbf{u})-R$ *represents the genuine difference between* T *and* R *after alignment, while* $T_c(\mathbf{u}) \approx R$ *so* $T_c(\mathbf{u}) - R$ *is correctly shown as* ≈ 0.

[20] B. Fischer and J. Modersitzki, *Ill-posed medicine - an introduction to image registration*, Inverse Problems, 24 (2008).
[21] A. Ghaffari and E. Fatemizadeh, *Image registration based on low rank matrix: Rank-regularized ssd*, IEEE transactions on medical imaging, 37 (2018), pp. 138–150.
[22] F. Gigengack, L. Ruthotto, M. Burger, C. H. Wolters, X. Jiang, and K. P. Schafers, *Motion correction in dual gated cardiac pet using mass-preserving image registration*, IEEE transactions on medical imaging, 31 (2012), pp. 698–712.
[23] A. Habbal, J. Petersson, and M. Thellner, *Multidisciplinary topology optimization solved as a nash game*, International Journal for Numerical Methods in Engineering, 61 (2004), pp. 949–963.
[24] S. Henn, *A multigrid method for a fourth-order diffusion equation with application to image processing*, SIAM Journal on Scientific Computing, 27 (2005), pp. 831–849.
[25] M. Ibrahim, K. Chen, and C. Brito-Loeza, *A novel variational model for image registration using gaussian curvature*, Geometry, Imaging and Computing, 1 (2015), pp. 417–446.
[26] M. Kallel, R. Aboulaich, A. Habbal, and M. Moakher, *A nash-game approach to joint image restoration and segmentation*, Applied Mathematical Modelling, 38 (2014), pp. 3038–3053.
[27] M. Kallel, M. Moakher, and A. Theljani, *The cauchy problem for a nonlinear elliptic equation: Nash-game approach and application to image inpainting*, Inverse Problems & Imaging, 9 (2015), pp. 853–874.
[28] S. L. Keeling, M. Hintermüller, F. Knoll, D. Kraft, and A. Laurain, *A total variation based approach to correcting surface coil magnetic resonance images*, Applied mathematics and computation, 218 (2011), pp. 219–232.
[29] Y. Kim and H. D. Tagare, *Intensity nonuniformity correction for brain mr images with known voxel classes*, SIAM Journal on Imaging Sciences, 7 (2014), pp. 528–557.
[30] D. Loeckx, P. Slagmolen, F. Maes, D. Vandermeulen, and P. Suetens, *Nonrigid image registration using conditional mutual information*, IEEE transactions on medical imaging, 29 (2010), pp. 19–29.
[31] A. Mang and G. Biros, *An inexact Newton–Krylov algorithm for constrained diffeomorphic image registration*, SIAM journal on imaging sciences, 8 (2015), pp. 1030–1069.
[32] A. Mang and G. Biros, *Constrained h^1-regularization schemes for diffeomorphic image registration*, SIAM Journal on Imaging Sciences, 9 (2016), pp. 1154–1194.
[33] J. Modersitzki, *FAIR: Flexible Algorithms for Image Registration*, SIAM, 2009.
[34] J. Modersitzki and S. Wirtz, *Combining homogenization and registration*, in International Workshop on Biomedical Image Registration, Springer, 2006, pp. 257–263.
[35] D. Monderer and L. S. Shapley, *Potential games*, Games and economic behavior, 14 (1996), pp. 124–143.
[36] J. Nash, *Equilibrium points in n-person games*, Proceedings of the National Academy of Sciences of the United States of America, 36 (1950), pp. 48–49.
[37] J. Nash, *Non-cooperative games*, Annals of mathematics, (1951), pp. 286–295.
[38] F. P. Oliveira and J. M. R. Tavares, *Medical image registration: a review*, Computer methods in biomechanics and biomedical engineering, 17 (2014), pp. 73–93.
[39] K. Papafitsoros, C. B. Schoenlieb, and B. Sengul, *Combined first and second order total variation inpainting using split bregman*, Image Processing On Line, 3 (2013), pp. 112–136.
[40] N. Parikh, S. Boyd, et al., *Proximal algorithms*, Foundations and Trends® in Optimization, 1 (2014), pp. 127–239.
[41] C. R. Park, K. Kim, and Y. Lee, *Development of a bias field-based uniformity correction in magnetic resonance imaging with various standard pulse sequences*, Optik, 178 (2019), pp. 161–166.
[42] S. Roy, A. Borzì, and A. Habbal, *Pedestrian motion modelled by fokker–planck nash games*, Royal Society open science, 4 (2017), p. 170648.
[43] A. Sotiras, C. Davatzikos, and N. Paragios, *Deformable medical image registration: A survey*, IEEE transactions on medical imaging, 32 (2013), pp. 1153–1190.
[44] K. Van Leemput, F. Maes, D. Vandermeulen, and P. Suetens, *Automated model-based bias field correction of mr images of the brain*, IEEE transactions on medical imaging, 18 (1999), pp. 885–896.
[45] U. Vovk, F. Pernus, and B. Likar, *A review of methods for correction of intensity inhomogeneity in mri*, IEEE transactions on medical imaging, 26 (2007), pp. 405–421.

[46] L. Wang and C. Pan, *Nonrigid medical image registration with locally linear reconstruction*, Neurocomputing, 145 (2014), pp. 303–315.
[47] C. Wu and X. C. Tai, *Augmented lagrangian method, dual methods, and split Bregman iteration for ROF, vectorial TV, and high order models*, SIAM Journal on Imaging Sciences, 3 (2010), pp. 300–339.
[48] C. Xing and P. Qiu, *Intensity-based image registration by nonparametric local smoothing*, IEEE Transactions on Pattern Analysis and Machine Intelligence, 33 (2011), pp. 2081–2092.
[49] W. Yilun, Y. Junfeng, Y. Wotao, and Z. Yin, *A new alternating minimization algorithm for total variation image reconstruction*, SIAM Journal on Imaging Sciences, 1 (2008), pp. 248–272.
[50] X. Zhen, X. Gu, H. Yan, L. Zhou, X. Jia, and S. B. Jiang, *Ct to cone-beam ct deformable registration with simultaneous intensity correction*, Physics in Medicine & Biology, 57 (2012), p. 6807.